Hepatocyte Notch activation induces liver fibrosis in non-alcoholic steatohepatitis

One Sentence Summary:

Aberrant hepatocyte Notch activation is required for development of non-alcoholic steatohepatitis-associated fibrosis, and Notch inhibition ameliorates obesity-induced liver disease.

Changyu Zhu[1], KyeongJin Kim[1], Xiaobo Wang[1], Alberto Bartolome[1], Marcela Salomao[2], Paola Dongiovanni[3], Marica Meroni[3], Mark J. Graham[4], Katherine P. Yates[5], Anna Mae Diehl[6], Robert F. Schwabe[1], Ira Tabas[1], Luca Valenti[3], Joel E. Lavine[7] and Utpal B. Pajvani[1]*

[1]Department of Medicine, Columbia University, New York, NY 10032, USA.

[2]Department of Pathology, Mayo Clinic, Phoenix, AZ 85054, USA.

[3]Department of Pathophysiology and Transplantation, Università degli Studi Milano, and Internal Medicine and Metabolic Diseases, Fondazione IRCCS Ca' Granda Ospedale Policlinico, Milan 20122, Italy.

[4]Ionis Pharmaceuticals, Inc., Carlsbad, CA 92010, USA.

[5]Department of Epidemiology, Johns Hopkins Bloomberg School of Public Health, Baltimore, MD 21205, USA.

[6]Division of Gastroenterology, Department of Medicine, Duke University Medical Center, Durham, NC 27710, USA.

[7]Department of Pediatrics, Columbia University, New York, NY 10032, USA.

*Corresponding author. Email: up2104@columbia.edu

Abstract

Fibrosis is the major determinant of morbidity and mortality in patients with non-alcoholic steatohepatitis (NASH), but has no approved pharmacotherapy in part due to incomplete understanding of its pathogenic mechanisms. Here, we report that hepatocyte Notch activity tracks with disease severity and treatment response in patients with NASH, and is similarly increased in a mouse model of diet-induced NASH and liver fibrosis. Hepatocyte-specific Notch loss-of-function mouse models showed attenuated NASH-associated liver fibrosis, demonstrating causality to obesity-induced liver pathology. Conversely, forced activation of hepatocyte Notch induced fibrosis in both chow- and NASH diet-fed mice by increasing Sox9-dependent Osteopontin expression and secretion from hepatocytes, which activate resident hepatic stellate cells. In a cross-sectional study, we found that Osteopontin explains the positive correlation between liver Notch activity and fibrosis stage in patients. Further, we developed a Notch inhibitor (*Nicastrin* anti-sense oligonucleotide, or *Ncst* ASO) that reduced fibrosis in NASH diet-fed mice. In sum, these studies demonstrate the pathological role and therapeutic accessibility of the maladaptive hepatocyte Notch response in NASH-associated liver fibrosis.

Introduction

Obesity and its metabolic consequences are among the most pressing public health challenges (*1, 2*). As the obese population-at-risk increases (*3*), the prevalence of obesity-related comorbidities such as non-alcoholic fatty liver disease (NAFLD), already the most common chronic liver disease (*4*), grows in parallel. NAFLD ranges in severity from simple steatosis (SS) to the hepatocellular injury and necroinflammatory changes which define non-alcoholic steatohepatitis (NASH), which predisposes patients to fibrosis and hepatocellular carcinoma (*5*). Whereas SS is considered a pre-disease state and NASH is potentially reversible (*6*), fibrosis severity is the main determinant of mortality in NAFLD patients (*7-10*). As organ availability for transplantation is already limited, new pharmaceutical targets to address NASH-associated fibrosis are a large unmet need for an increasingly obese population.

The Notch family of transmembrane receptors (Notch1-4) determines cell fate during development (*11*) through ligand binding and γ-secretase-mediated cleavage which generates Notch intracellular domain (NICD) (*12*), which binds Rbp-Jκ and Mastermind (MAM) to activate transcription of canonical Notch targets including the *Hairy enhancer of split* (*Hes*) and *Hes-related* (*Hey*) family genes (*13*). In liver, Notch activation pushes hepatic progenitor cells' differentiation to cholangiocytes and formation of the biliary tree, whereas Notch-inactive progenitors commit to hepatocyte lineage (*14*), which sets the quiescent baseline of Notch signaling in hepatocytes in normal liver. However, we found liver Notch activity is increased in obese rodents (*15*) and in patients with SS or NASH (*16*), although the relative contributions of hepatocyte and nonparenchymal cell (NPC) Notch activity were unclear.

Here, we found that the number of HES1+ hepatocytes, but not NPCs, is increased in patients with NASH. In longitudinal analysis using paired baseline and end-of-treatment biopsy specimens from the Pioglitazone versus Vitamin E versus Placebo for the Treatment of Nondiabetic Patients with Non-alcoholic Steatohepatitis (PIVENS) trial (*17, 18*), we found that Notch activity, specifically in hepatocytes, tracks with NASH severity. These data suggested that hepatocyte Notch activation may be a biomarker or a causal determinant of NASH severity. To distinguish these possibilities, we used a palmitate/cholesterol-rich diet coupled with fructose-containing drinking water (*19*) fed to wildtype (WT)

mice to induce NASH/fibrosis, which increased hepatocyte but not NPC Notch activation. Two genetic hepatocyte-specific Notch loss-of-function mouse models showed lower hepatic stellate cell (HSC) activity and liver collagen deposition without changes in hepatocellular injury or inflammation, whereas forced activation of hepatocyte Notch induced fibrosis in chow-fed mice due to Sox9-dependent expression of *Spp1* (encoding the secreted fibrogenic factor Osteopontin). Treating NASH diet-fed WT mice with a Notch antagonist (*Ncst* ASO) decreased liver fibrosis. In sum, these data support the necessity and therapeutic tractability of hepatocyte Notch signaling for the development of NASH-associated liver fibrosis.

Results

Hepatocyte Notch activity tracks with NASH severity in patients

Steady-state liver Notch activation is associated with higher serum alanine aminotransferase (ALT) and NAFLD activity score (NAS), biochemical and pathologic markers of NASH, independent of steatosis or insulin resistance (*16*). To test relative hepatocyte and NPC contribution, we stained liver biopsy specimens taken at time of bariatric surgery from patients with pathologically normal livers, SS, or NASH/fibrosis**.** We observed detectable basal NPC expression of HES1, which although modestly increased in SS, did not further change in NASH/fibrosis (**Fig. 1A** and **fig. S1**). Hepatocyte HES1, however, was nearly absent in normal livers, mildly elevated in SS, but highly increased in patients with NASH/fibrosis (**Fig. 1A**).

Next, to determine whether liver Notch activity may co-vary with NASH severity and treatment response, we performed parallel cross-sectional and longitudinal analyses in samples derived from the PIVENS trial. PIVENS investigators randomized adult, non-diabetic patients with NASH to placebo, vitamin E (800 IU daily), or pioglitazone (30mg daily) arms, taking liver biopsies at enrollment and end-of-treatment (96-week) visits (*20*). A “Responder” was defined as an NAS response of at least 2 points, or resolution of NASH. In cross-sectional analysis of 118 samples (**table S1**), Responders showed lower liver Notch activity than Non-responders at the end of the trial (**Fig. 1B**). Next, in longitudinal analysis from a subset of PIVENS subjects that had paired baseline and end-of-treatment cDNA (**table S1**), we found a reduction from baseline *HES1* and *HEYL* expression in Responders but not Non-responders (**Fig. 1, C** and **D**). Finally, we found reduced hepatocyte, but not NPC, HES1 staining in liver sections from PIVENS Responders from baseline and as compared to Non-responders (**Fig. 1E**). In sum, these data suggest that liver Notch activity, specifically in hepatocytes, tracks with NASH disease severity.

Hepatocyte Notch activity is increased in a mouse model of diet-induced NASH

As a first step towards determining if a causal relationship exists between Notch activity and NASH, we fed WT C57BL/6J mice a NASH-provoking diet for 16 weeks, which induced hepatic steatosis, inflammation, and fibrosis as compared to chow-fed mice (**fig. S2**) (*19*). As in patients with NASH/fibrosis, we found higher liver and hepatocyte, but not NPC, *Hes1* in NASH diet-fed mice (**Fig. 1F**), reflecting an increased number of Hes1+ hepatocytes and increased Hes1 staining intensity per cell (**Fig. 1G**), consistent with increased expression and activation of *Notch1* and *Notch2* (**Fig. 1, H** and **I**). In parallel, using a Notch reporter mouse that expresses the fluorescent protein Venus under the control of four Rbp-jκ binding sites (*21*), we found a large increase in Venus+ hepatocytes in NASH diet-fed mice (**Fig. 1J**).

Hepatocyte Notch mediates NASH diet-induced liver fibrosis

The positive correlations between hepatocyte Notch activation and NASH severity provided the impetus to generate hepatocyte-specific Notch loss-of-function mice to test causality to the phenotype. As the Mastermind (MAM) transcriptional co-activator is downstream of all four Notch receptors, we transduced mice with a dominant-negative MAM (DNMAM) allele (*22*) in the *Rosa26* locus (*Rosa*^{DNMAM}) with AAV8-*Tbg-Cre*, to take advantage of liver tropism of AAV8 and the hepatocyte-specific thyroxine binding globulin (*Tbg*) promoter (*23, 24*). This approach generated mice with post-development hepatocyte-specific expression of DNMAM (*L-DNMAM* mice, **Fig. 2A**). After 16 weeks of NASH diet, *L-DNMAM* mice showed similar body weight and adiposity (**fig. S3, A** and **B)** as compared with control *Rosa*^{DNMAM} mice transduced with AAV8-TBG-*LacZ*, but lower liver *Hes1* expression (**Fig. 2B**), fewer Hes1+ hepatocytes, and weaker Hes1 staining intensity per cell (**Fig. 2C** and **fig. S3C**). Despite unchanged liver lipid accumulation, TUNEL staining, inflammatory gene expression, CD45+ infiltrate, and serum transaminases (**Fig. 2D; fig. S3, D** to **I**)**,** markers of HSC activation (*Col1a1*, *Acta2*, and *Timp1*) were decreased (**Fig. 2E**), which translated to less collagen deposition in *L-DNMAM* livers (**Fig. 2F**).

Next, to ensure reproducibility of these results, we ablated hepatocyte *Nicastrin* (*25*), the γ-secretase targeting subunit necessary for ligand-dependent Notch activation (*L-Ncst* mice) (*26*). Similar

to *L-DNMAM* mice, NASH diet-fed *L-Ncst* mice showed normal body weight and adiposity (**fig. S4, A** and **B**), but reduced hepatic *Hes1* (**fig. S4C**) and fibrogenic gene expression (**fig. S4D**), and a tendency towards less fibrosis (**fig. S4E**) as compared to Cre- controls, despite unchanged hepatic TUNEL staining or serum transaminases, liver inflammation, and only minor changes in liver lipid content (**fig. S4, F** to **L**).

These data suggest that hepatocyte Notch signaling is necessary for the full development of NASH diet-induced fibrosis. To test whether a late inhibition of Notch in hepatocytes may ameliorate NASH-associated fibrosis, we fed adult *Rosa*^{DNMAM} mice the NASH diet for 16 weeks prior to AAV8-*Tbg-Cre* transduction (**Fig. 2G**). In this experimental paradigm, we again observed decreased liver *Hes1* (**Fig. 2H**) and a parallel reduction in HSC-mediated liver fibrosis (**Fig. 2, I** and **J**), despite unchanged body weight, adiposity, liver steatosis, inflammation, TUNEL staining or serum transaminases (**fig. S5, A** to **I**). These data indicate that inhibition of hepatocyte Notch signaling can interrupt NASH-associated fibrosis even after fibrosis has begun to develop.

Hepatocyte Notch is not required for MCD diet-induced fibrosis

Acute toxin exposure increases Notch activity in HSCs and immune cells (*27-29*), contrary to what we find in FACS-purified HSCs and myeloid cells isolated from NASH diet-fed mice (**fig. S6A**). Similarly, we observed that methionine-choline deficient (MCD) diet, which induces severe liver injury, inflammation, and fibrosis in addition to anorexia and rapid weight loss (*30, 31*), led to increased liver *Hes1* expression relative to chow-fed controls (**fig. S6B**). This increased Hes1 expression was predominantly seen in NPCs (**fig. S6C**), unlike in NASH diet-feeding (**fig. S6D**). These data are consistent with a recent study showing unchanged expression of Notch targets in hepatocytes in MCD-fed mice (*32*), as well as our finding that MCD diet-fed *L-DNMAM* mice show no difference in liver *Hes1* and fibrogenic gene expression or collagen deposition (**fig. S6, E** to **H**), suggesting specificity of the hepatocyte Notch response in NASH.

Forced hepatocyte Notch activation exacerbates diet-induced NASH and fibrosis

We next evaluated whether forced hepatocyte Notch activation by AAV8-TBG-*Cre* transduction of mice that carry a Cre-inducible constitutively-active (*Rosa*^{NICD}) Notch1 (*33*) may exacerbate NASH/fibrosis (*L-NICD*-16wks, **Fig. 3A**). In parallel, because 8 weeks of NASH diet provokes steatosis but no apparent fibrosis (*19*), we transduced *Rosa*^{NICD} mice with AAV8-TBG-*Cre* halfway through the diet study (*L-NICD*-8wks, **Fig. 3A**) to determine if hepatocyte Notch activity promotes the transition from steatosis to NASH/fibrosis. As compared to AAV8-TBG-*LacZ*-transduced *Rosa*^{NICD} controls, both *L-NICD* groups showed a mild (~2-fold) increase in liver *Hes1* due to increased Hes1+ hepatocyte number and cellular Hes1 content (**Fig. 3, B** and **C**; **fig. S7A**), as well as increased HSC activation and pericellular collagen deposition (**Fig. 3, D** and **E**), even with a mild decrease of liver triglyceride (**fig. S7, B and C**). Hepatocyte Notch gain-of-function also did not change hepatocellular death (**Fig. 3F**), underscoring the predominant effects of hepatocyte Notch activation on liver fibrosis development, but did show enhanced liver inflammation and CD45+ immune cell infiltration (**fig. S7, D** and **E**).

Although NASH is prevalent in both male and female humans (*34*), female mice tend to be protected from diet-induced obesity and consequent metabolic complications. Consistent with their male counterparts, despite unchanged body weight and adiposity (**fig. S7, F** and **G**), female *L-NICD* mice showed increased liver *Hes1*, inflammatory and fibrogenic gene expression (**fig. S7, H** to **J**), and exacerbated liver inflammation and fibrosis as compared to AAV8-TBG-*LacZ*-transduced controls (**fig. S7, K** and **L**).

Hepatocyte Notch activation causes liver fibrosis in the absence of steatohepatitis

NASH is associated with simultaneous pathologic insults: lipotoxicity, hepatocellular injury, inflammation and fibrosis. Each hit may affect development and/or progression of the others (*35, 36*); for example, lipotoxicity-induced hepatocellular injury contributes to HSC activation (*37, 38*). Although we observed unchanged hepatocellular death in Notch loss- or gain-of-function mice, it is difficult to disentangle the effects of hepatocyte Notch on liver fibrosis from other changes associated with an obesogenic diet. However, even lean, chow-fed *L-NICD* male mice (**Fig. 4A** and **fig. S8, A** to **C**), without apparent hepatocellular injury (**Fig. 4B** and **fig. S8, D** and **E**), showed increased liver

inflammation (**fig. S8, F** and **G**), fibrogenic gene expression (**Fig. 4C**), and greater collagen deposition (**Fig. 4D**) than Cre- controls. This phenotype was recapitulated in *L-NICD* female mice (**fig. S9**). These data suggest that hepatocyte Notch activation is sufficient to trigger HSC activation and liver fibrosis even in the absence of liver steatosis or hepatocyte injury.

Loss of hepatocyte Notch activity does not affect ductular reactions

Notch activation in hepatocytes may promote transdifferentiation to a cholangiocyte lineage (*23, 39*), contributing to ductular reaction (DR). As DR and liver fibrosis frequently co-exist (*40-43*), we hypothesized that Notch-induced liver fibrosis may depend on Notch-induced DR. NASH diet induced ductular proliferation, as evidenced by increased liver *Krt19* expression and number of Cytokeratin 19-positive (CK19+) cells (**fig. S10, A** and **B**), which was exacerbated in *L-NICD* mice (**fig. S10, C** and **D**). Further, as previously observed (*23*), a subset of *L-NICD* hepatocytes adopted a biliary fate (**fig. S10E**). However, NASH diet-fed Notch loss-of-function mice showed comparable DR to controls (**fig. S10, F** and **G**). These data suggest that constitutive Notch overexpression can induce hepatocyte transdifferentiation, but hepatocyte Notch activation is not necessary for NASH-diet induced DR which likely derives from cholangiocytes.

Notch-induced Sox9 activates hepatocyte *Spp1* expression

We next considered alternative explanations for the robust effect of hepatocyte Notch on liver fibrosis, and hypothesized that Notch-active hepatocytes may secrete fibrogenic factor(s) that activate HSCs (*44*). Indeed, conditioned medium (CM) collected from primary hepatocytes transduced with Ad-NICD stimulated greater activation of primary HSCs as compared to Ad-GFP-transduced hepatocyte CM (**Fig. 4E**). Intriguingly, Notch activation did not globally affect the secretome, but elevated secretion of the fibrogenic factor Osteopontin (**fig. S11A**), likely due to increased *Spp1* expression (**Fig. 4F**). Although Osteopontin is known to activate HSCs (*45-48*), hepatocyte-derived Osteopontin has not been well-described. We found that *Spp1* was increased in hepatocytes derived from NASH diet-fed WT mice (**Fig. 4G**), with a preferential increase in Venus+ hepatocytes in Notch reporter mice (**Fig. 4H**).

Thus, NASH diet-fed *L-DNMAM* mice showed lower *Spp1* as compared to Cre- controls (**Fig. 4I**), whereas *Spp1* expression was markedly increased in chow- or NASH diet-fed *L-NICD* mice (**Fig. 4J** and **fig. S11, B** and **C**). This regulation appeared fairly specific – similar to results from the cytokine array, expression of other secreted fibrogenic factors (Hedgehog, TGFβ and PDGFs) were not Notch-activated in hepatocytes (**fig. S11D**) and/or do not show reciprocal reduction with Notch loss-of-function (**fig. S11E**).

These data suggest a cell-autonomous effect of hepatocyte Notch activation on *Spp1* transcription. As the *Spp1* promoter does not possess a consensus Rbp-Jk binding sequence, we identified additional candidates – Sox9 (Sex determining region Y-Box 9), a direct Notch transcriptional target (*49*), which we observed to track with genetic manipulations of Notch signaling (**fig. S11, F** to **I**), and Hes1, which has been suggested to regulate *Spp1* expression in osteoblasts (*50*). To distinguish between these candidate mechanisms, we used siRNA to knock down *Hes1* or *Sox9* expression and found that only siRNA directed to *Sox9* blunted NICD-induced *Spp1* (**Fig. 4K**), suggesting Sox9 is the transcriptional mediator of Notch-induced *Spp1* expression in hepatocytes.

Notch-mediated Osteopontin secretion from hepatocytes activates HSCs to induce liver fibrosis

To determine whether increased Osteopontin secretion may explain HSC activation induced by hepatocyte Notch activation, we transfected hepatocytes with siRNA to *Spp1* (**Fig. 5, A** and **B; fig. S11J**), which abrogated HSC activation induced by Ad-NICD hepatocyte CM (**Fig. 5C**). In a parallel approach, we pre-treated CM with an Osteopontin neutralizing antibody before addition to HSCs, which similarly negated Notch-induced fibrogenic gene expression (**Fig. 5D**).

Next, we generated AAV8-H1-sh*Spp1* to silence hepatocyte *Spp1*, and transduced adult NASH diet-fed $Rosa^{NICD}$ mice with AAV8-TBG-*Gfp* or –*Cre*, with or without simultaneous *Spp1* knockdown (**Fig. 5E**). AAV8-H1-sh*Spp1* transduction did not affect body weight, adiposity, *Hes1* expression, liver injury or inflammatory gene expression (**fig. S12, A** to **F**), but successfully attenuated Notch-induced hepatocyte *Spp1* without affecting cholangiocyte Osteopontin (**Fig. 5F** and **fig. S12, G** and **H**).

Consistent with in vitro experiments, preventing Notch-induced hepatocyte *Spp1* expression nearly normalized increased fibrogenic gene expression (**Fig. 5G**) and excess collagen deposition seen in NASH diet-fed *L-NICD* mice (**Fig. 5H**).

To test the clinical importance of this observation, we analyzed expression of hepatic *SPP1* and *HES1* in 159 patients undergoing percutaneous liver biopsy for suspected NASH (**Ttable S2**). We observed a strong concordance between *HES1* and *SPP1* (**Fig. 5I**). Moreover, when we performed multivariate regression analysis to adjust for potential demographic, metabolic and genetic confounders, *HES1* was significantly (P = 0.016) and positively correlated with fibrosis stage, but not when *SPP1* was added into the regression model (**Fig. 5J**). In combination with our mechanistic experiments in vitro and associated mouse modeling, these data suggest that Notch-induced HSC activation and liver fibrosis is likely Osteopontin-dependent.

Pharmacologic Notch inhibition ameliorates NASH-associated liver fibrosis

Notch inhibitors are in clinical trials for cancer (*51*) – the most commonly studied of these are γ-secretase inhibitors (GSIs) (*52*) that block endogenous production of NICD. We have previously shown that dibenzazepine, a well-characterized and bioavailable GSI (*53*), can potently inhibit Notch signaling in vivo (*15, 54*). To test whether acute Notch inhibition can ameliorate NASH-associated liver fibrosis, we treated WT mice with GSI or vehicle once daily for 1 week, initiating treatment after nearly 4 months of NASH diet. Acute GSI treatment did not alter body weight, adiposity or liver inflammation (**fig. S13, A** to **E**), but as expected from our genetic models, lowered liver Notch activity, *Spp1* (**fig. S13F**) and fibrogenic gene expression (**fig. S13G**), with only a trend towards less fibrosis (**fig. S13H**). These data imply that 1 week of GSI exposure is insufficient to reverse liver fibrosis, so next we used a chronic, intermittent dosing strategy at lower GSI dose to mitigate potential toxicity (**Fig. 6A**). As previously observed (*55*), chronic GSI treatment lowered body weight, adiposity, and liver Notch activity (**fig. S14, A** and **B**, **Fig. 6B**), and was sufficient to reduce HSC activation and liver fibrosis (**Fig. 6, C** and **D**), without effects on inflammation (**fig. S14, C** and **D**).

Unfortunately, chronic GSI treatment induces goblet cell metaplasia (*53*), even at the lower dose we used here (**fig. S14E**). Resultant intestinal toxicity likely precludes repurposing GSIs for NASH. Thus, we developed a liver-selective γ-secretase antagonist to bypass intestinal distribution – *Ncst* anti-sense oligonucleotide (ASO) (*26*). Based on pre-clinical data with ASOs of similar chemistry (*56-58*), we predicted once-weekly *Ncst* ASO would be well-tolerated and effectively block liver Notch signaling as compared to control ASO. Indeed, weekly *Ncst* ASO dosing of NASH diet-fed WT mice (**Fig. 6E**) reduced liver *Nicastrin*, Notch activity, and *Spp1* expression (**Fig. 6F**) as compared to control ASO-treated mice. *Ncst* ASO did not affect liver TUNEL staining (**Fig. 6G**), serum transaminases or liver inflammation (**fig. S14, F** to **I**), but effectively reduced expression of HSC markers and collagen deposition (**Fig. 6, H** and **I**). *Ncst* ASO lowered body weight and adiposity (**fig. S14, J** and **K**), likely due to adipose ASO uptake (*59*), but showed no intestinal toxicity (**fig. S14L**), in contrast to chronic GSI dosing. Control ASO had no effect (**fig. S15**). These proof-of-principle studies echo data from Notch loss-of-function mice, suggesting that hepatocyte Notch activation is central to development of obesity-induced liver fibrosis and may be therapeutically targeted in NASH (fig. S16).

Discussion

Fibrosis, although not a diagnostic determinant of NASH, predisposes to cirrhosis and liver malignancy and is the major determinant of long-term mortality of NASH patients (*8-10*). NASH is projected to be the leading cause of liver transplantation due to lack of approved therapeutics (*60, 61*), underscoring the urgency to uncover mechanisms of NASH-induced fibrosis to find targetable pathways. Our study demonstrates that hepatocyte Notch signaling is virtually absent in normal liver, but tracks with NASH severity in mouse and man, and is maladaptive, leading ultimately to Osteopontin secretion and liver fibrosis. Osteopontin is a known regulator of HSC activation, but the contribution of hepatocyte-derived Osteopontin in NASH suggests that Notch-activated hepatocytes are not simple bystanders but rather alter the liver microenvironment to potentiate fibrosis.

To place our work in context, although several studies have suggested increased Notch activity in NPCs with CCl_4-induced acute liver injury (*27, 29*), none have linked hepatocyte Notch to fibrosis in the setting of NASH. We hypothesize that CCl_4 treatment or MCD diet-feeding provokes rapid hepatocellular death (*27, 32*), which induces Notch activation in inflammatory cells and HSCs as part of a proliferative injury response. But these stimuli provoke minimal and/or non-sustained hepatocyte Notch activation – thus, hepatocyte-specific Notch inhibition has no impact on liver fibrosis in MCD diet-fed mice. On the contrary, in the low-grade but long-term injury associated with obesity/insulin-resistance seen in NASH diet-fed mice (and in human NASH), hepatocyte Notch activity is specifically increased to cope with the chronic insult. Our proof-of-principle experiments with *Ncst* ASO highlight the potential of Notch-directed therapeutics to address NASH-associated fibrosis without the intestinal toxicity associated with systemic Notch inhibition (GSIs). However, as liver-targeted Notch antagonism may be fraught with side effects including disruption of hepatic vascular integrity (*62*), GalNAc-modified siRNA (*63, 64*) or nanoparticle strategies (*65*) retain great potential to address the inappropriate hepatocyte Notch activity in NASH patients without affecting normal Notch activity in liver NPCs and other tissues.

Our data show that hepatocyte Notch-mediated Osteopontin secretion can directly activate HSCs, independent of hepatocellular injury, leading to excessive collagen deposition. But our

data also points to other possible paths of increased fibrosis with hepatocyte Notch activity. For instance, a subset of *L-NICD* hepatocytes adopted a biliary fate, consistent with Notch's role in bile duct development (*14*) and ability to promote transdifferentiation to a biliary fate (*23*). Although DR arises primarily from cholangiocytes in liver injury (*66*), as DR is associated with liver fibrosis (*40-43*), Notch-induced hepatocyte cell fate change may augment fibrosis in *L-NICD* mice. Hepatocyte secretion of Osteopontin, normally a biliary marker, in response to Notch activation may suggest an incomplete transition of hepatocytes towards biliary fate. Notch loss-of-function mice, however, show unchanged DR as assessed by CK19+ cell number, but still less fibrosis than controls; further, a specific knockdown of hepatocyte Osteopontin reduces fibrosis in *L-NICD* mice. Thus, our data support the conclusion that hepatocyte Notch activity facilitates liver fibrosis in NASH by both direct (Osteopontin-mediated HSC activation) as well as possibly indirect (inflammation, DR) pathways.

There are several limitations of our study. For instance, our conclusions were derived primarily with the use of a NASH-provoking diet. Although we saw robust and reproducible diet-induced obesity, liver inflammation, and fibrosis across cohorts, additional studies are necessary to determine whether this diet accurately models NASH pathogenesis. Further, there may be additional Notch-regulated factors involved in the pathogenesis of NASH/fibrosis yet to be identified, and future work is necessary to isolate the upstream signal leading to hepatocyte Notch activation in NASH. Finally, although we find an association between hepatocyte Notch activation and NASH severity and therapeutic outcome in patients, it is important to recognize that all intervention studies were performed in mouse models, and the potential translational relevance of Notch inhibitors in human NASH and fibrosis requires formal testing. Nevertheless, we believe these data provide strong impetus to develop hepatocyte-specific Notch inhibitors to treat the burgeoning health crisis of NASH-associated fibrosis.

Materials and Methods

Study design. The objective of this study was to 1) determine what cell type in liver is responsible for increased Notch activation seen in patients with NASH; 2) define what role Notch activation plays in NASH-associated fibrosis development, by combining a dietary mouse model of NASH with Notch loss- (*L-DNMAM* and *L-Ncst*) and gain-of-function (*L-NICD*) transgenic mice; 3) define the fibrogenic machinery downstream of hepatocyte Notch activation by co-culture of primary hepatocytes and stellate cells in vitro, AAV-mediated knockdown approach in vivo with validation from translational studies in patients with NASH; and 4) determine if pharmacologic Notch inhibition can ameliorate NASH-induced fibrosis in mice.

All data presented have been replicated in independent cohorts of mice or at least 3 biological replicates for in vitro experiments, with all staining data quantitatively analyzed by Zen software. Statistical significance was performed by Student's *t* test, or ANOVA followed by post-hoc *t* tests for multiple comparisons. Based on predicted effects of Notch activation on various pathologic metrics in mice, with a power of 0.8 and $P < 0.05$, we calculated a sample size necessary of between 6 to 11 mice per group. Animals were randomly allocated into control and experimental groups, with group assignment recorded in a master spreadsheet and only unmasked when all samples of the respective experiments were analyzed. Human samples were obtained from a completed randomized, controlled trial (PIVENS), or a cross-sectional study for which randomization was not applicable – group assignments and other demographic information were blinded to the investigators until after all data were obtained. Data collection of each experiment was detailed in the respective figures, figure legends, and methods. No data were excluded from studies in this manuscript.

Human liver biopsies

Cross-sectional HES1 staining. Normal (n = 3), SS (n = 3) and NASH liver (n = 4) sections were obtained from morbidly obese individuals who underwent liver biopsy at time of bariatric surgery to assess liver histopathology. The protocol was approved by the Ethical Committee of the Fondazione IRCCS of Milan, and each patient signed a written informed consent.

PIVENS trial. We analyzed liver gene expression of *HES1* and *HEYL* and performed immunostaining of HES1 and HNF4α using liver biopsy samples from PIVENS trial. PIVENS is a NASH treatment trial sponsored by NIDDK and conducted by the Nonalcoholic Steatohepatitis Clinical Research Network (NASH CRN). The PIVENS trial study design has been described and the ClinicalTrials.gov identifier is NCT00063622.

Cross-sectional gene expression analysis in patients with suspected NASH. We analyzed liver gene expression of *HES1* and *SPP1* in individuals who underwent liver biopsy for suspected NASH, due to the presence of persistent elevations in liver enzymes or due to severe obesity (*67*). The protocol was approved by the Ethical Committee of the Fondazione IRCCS of Milan, and each patient signed a written informed consent. For statistical analysis, comparisons were made by fitting data to generalized linear models, unadjusted (univariate analyses), or considering as independent variables: age, gender, BMI, presence of impaired fasting glucose or T2D. Hepatic *HES1* and *SPP1* mRNA expression were normalized to *ACTB* expression and natural log transformed before analyses to ensure a normal distribution.

Animal studies. Homozygous *Rosa*^{DNMAM} (*22*), *Rosa*^{NICD} (*33*), and Notch-Venus (*21*) male mice were crossed with female C57BL/6J (Jackson Labs, strain #000664) mice to generate heterozygous transgenic mice for experiments. *Nicastrin*$^{flox/flox}$ mice (*25*) were crossed with Albumin-*Cre* mice (*68*) to generate *L-Ncst* mice. All strains were maintained on C57BL/6J genetic background. Mice were weaned to standard chow (Picolab rodent diet 20, #5053) for all experiments, then started on NASH diet (Teklad, TD.160785) with fructose-containing drinking water (23.1 g fructose and 18.9 g glucose dissolved in 1 L water, then filter-sterilized) or MCD diet (Dyets, #518810GI) at 8 weeks of age, unless otherwise noted. Animals were housed in standard cages at 22°C in a 12 hr light/12 hr dark cycle, and monitored for overall well-being and signs of distress with body weight measured weekly. Upon completion of each studies, all mice were weighed and euthanized. Blood was collected via cardiac puncture. Perigonadal adipose tissues were removed and weighed. Livers were weighed, excised and

split for fixation, RNA and protein isolation, and frozen for future analyses. The Columbia University Institutional Animal Care and Use Committee approved all animal procedures.

Statistical analysis. Results are shown as mean ± s.e.m unless indicated otherwise. Statistical analysis was performed using Prism software (version 6, GraphPad Software). Differences between 2 groups were calculated using a 2-tailed Student's *t* test. Analysis involving multiple groups was performed using one-way ANOVA followed by post-hoc *t* tests. Risk factors for fibrosis severity (stage 0-4) in patients were evaluated by multivariate ordinal regression analysis. *HES1* and *SPP1* expression in the cross-sectional study were log transformed to ensure the assumption of normal distribution. $P < 0.05$ was considered statistically significant.

Supplementary Materials

References and Notes:

1. P. Hossain, B. Kawar, M. El Nahas, Obesity and diabetes in the developing world--a growing challenge. *The New England journal of medicine* **356**, 213-215 (2007); published online EpubJan 18 (10.1056/NEJMp068177).
2. M. Lazo, J. M. Clark, The epidemiology of nonalcoholic fatty liver disease: a global perspective. *Seminars in liver disease* **28**, 339-350 (2008); published online EpubNov (10.1055/s-0028-1091978).
3. C. L. Ogden, M. D. Carroll, C. D. Fryar, K. M. Flegal, Prevalence of Obesity Among Adults and Youth: United States, 2011-2014. *NCHS data brief*, 1-8 (2015); published online EpubNov (
4. Z. M. Younossi, M. Stepanova, M. Afendy, Y. Fang, Y. Younossi, H. Mir, M. Srishord, Changes in the prevalence of the most common causes of chronic liver diseases in the United States from 1988 to 2008. *Clin Gastroenterol Hepatol* **9**, 524-530.e521; quiz e560 (2011); published online EpubJun (10.1016/j.cgh.2011.03.020).
5. E. M. Brunt, Pathology of nonalcoholic fatty liver disease. *Nature reviews. Gastroenterology & hepatology* **7**, 195-203 (2010); published online EpubApr (10.1038/nrgastro.2010.21).
6. S. Gawrieh, N. Chalasani, Pharmacotherapy for Nonalcoholic Fatty Liver Disease. *Semin Liver Dis* **35**, 338-348 (2015); published online EpubAug (10.1055/s-0035-1562951).
7. D. Kim, W. R. Kim, H. J. Kim, T. M. Therneau, Association between noninvasive fibrosis markers and mortality among adults with nonalcoholic fatty liver disease in the United States. *Hepatology* **57**, 1357-1365 (2013); published online EpubApr (10.1002/hep.26156).
8. P. S. Dulai, S. Singh, J. Patel, M. Soni, L. J. Prokop, Z. Younossi, G. Sebastiani, M. Ekstedt, H. Hagstrom, P. Nasr, P. Stal, V. W. Wong, S. Kechagias, R. Hultcrantz, R. Loomba, Increased risk of mortality by fibrosis stage in nonalcoholic fatty liver disease: Systematic review and meta-analysis. *Hepatology* **65**, 1557-1565 (2017); published online EpubMay (10.1002/hep.29085).
9. P. Angulo, D. E. Kleiner, S. Dam-Larsen, L. A. Adams, E. S. Bjornsson, P. Charatcharoenwitthaya, P. R. Mills, J. C. Keach, H. D. Lafferty, A. Stahler, S. Haflidadottir, F. Bendtsen, Liver Fibrosis, but No Other Histologic Features, Is Associated With Long-term Outcomes of Patients With Nonalcoholic Fatty Liver Disease. *Gastroenterology* **149**, 389-397 e310 (2015); published online EpubAug (10.1053/j.gastro.2015.04.043).
10. M. Ekstedt, H. Hagstrom, P. Nasr, M. Fredrikson, P. Stal, S. Kechagias, R. Hultcrantz, Fibrosis stage is the strongest predictor for disease-specific mortality in NAFLD after up to 33 years of follow-up. *Hepatology* **61**, 1547-1554 (2015); published online EpubMay (10.1002/hep.27368).
11. M. E. Fortini, D. Bilder, Endocytic regulation of Notch signaling. *Current opinion in genetics & development* **19**, 323-328 (2009); published online EpubAug (10.1016/j.gde.2009.04.005).
12. B. De Strooper, Nicastrin: gatekeeper of the gamma-secretase complex. *Cell* **122**, 318-320 (2005); published online EpubAug 12 (10.1016/j.cell.2005.07.021).
13. V. Bolos, J. Grego-Bessa, J. L. de la Pompa, Notch signaling in development and cancer. *Endocrine reviews* **28**, 339-363 (2007); published online EpubMay (10.1210/er.2006-0046).
14. Y. Zong, B. Z. Stanger, Molecular mechanisms of liver and bile duct development. *Wiley interdisciplinary reviews. Developmental biology* **1**, 643-655 (2012); published online EpubSep-Oct (10.1002/wdev.47).
15. U. B. Pajvani, C. J. Shawber, V. T. Samuel, A. L. Birkenfeld, G. I. Shulman, J. Kitajewski, D. Accili, Inhibition of Notch signaling ameliorates insulin resistance in a FoxO1-dependent manner. *Nat Med* **17**, 961-U978 (2011); published online EpubAug (Doi 10.1038/Nm.2378).
16. L. Valenti, R. M. Mendoza, R. Rametta, M. Maggioni, C. Kitajewski, C. J. Shawber, U. B. Pajvani, Hepatic notch signaling correlates with insulin resistance and nonalcoholic fatty liver disease. *Diabetes* **62**, 4052-4062 (2013); published online EpubDec (10.2337/db13-0769).
17. A. J. Sanyal, N. Chalasani, K. V. Kowdley, A. McCullough, A. M. Diehl, N. M. Bass, B. A. Neuschwander-Tetri, J. E. Lavine, J. Tonascia, A. Unalp, M. Van Natta, J. Clark, E. M. Brunt, D. E. Kleiner, J. H. Hoofnagle, P. R. Robuck, C. R. N. Nash, Pioglitazone, vitamin E, or placebo for nonalcoholic steatohepatitis. *The New England journal of medicine* **362**, 1675-1685 (2010); published online EpubMay 6 (10.1056/NEJMoa0907929).

18. N. P. Chalasani, A. J. Sanyal, K. V. Kowdley, P. R. Robuck, J. Hoofnagle, D. E. Kleiner, A. Unalp, J. Tonascia, Pioglitazone versus vitamin E versus placebo for the treatment of non-diabetic patients with non-alcoholic steatohepatitis: PIVENS trial design. *Contemporary clinical trials* **30**, 88-96 (2009); published online EpubJan (10.1016/j.cct.2008.09.003).
19. X. Wang, Z. Zheng, J. M. Caviglia, K. E. Corey, T. M. Herfel, B. Cai, R. Masia, R. T. Chung, J. H. Lefkowitch, R. F. Schwabe, I. Tabas, Hepatocyte TAZ/WWTR1 Promotes Inflammation and Fibrosis in Nonalcoholic Steatohepatitis. *Cell Metab* **24**, 848-862 (2016); published online EpubDec 13 (10.1016/j.cmet.2016.09.016).
20. D. E. Kleiner, E. M. Brunt, M. Van Natta, C. Behling, M. J. Contos, O. W. Cummings, L. D. Ferrell, Y. C. Liu, M. S. Torbenson, A. Unalp-Arida, M. Yeh, A. J. McCullough, A. J. Sanyal, N. Nonalcoholic Steatohepatitis Clinical Research, Design and validation of a histological scoring system for nonalcoholic fatty liver disease. *Hepatology* **41**, 1313-1321 (2005); published online EpubJun (10.1002/hep.20701).
21. S. Nowotschin, P. Xenopoulos, N. Schrode, A.-K. Hadjantonakis, A bright single-cell resolution live imaging reporter of Notch signaling in the mouse. *BMC Developmental Biology* **13**, 15 (2013)10.1186/1471-213x-13-15).
22. L. Tu, T. C. Fang, D. Artis, O. Shestova, S. E. Pross, I. Maillard, W. S. Pear, Notch signaling is an important regulator of type 2 immunity. *J Exp Med* **202**, 1037-1042 (2005); published online EpubOct 17 (10.1084/jem.20050923).
23. K. Yanger, Y. Zong, L. R. Maggs, S. N. Shapira, R. Maddipati, N. M. Aiello, S. N. Thung, R. G. Wells, L. E. Greenbaum, B. Z. Stanger, Robust cellular reprogramming occurs spontaneously during liver regeneration. *Genes Dev* **27**, 719-724 (2013); published online EpubApr 01 (10.1101/gad.207803.112).
24. X. Mu, R. Espanol-Suner, I. Mederacke, S. Affo, R. Manco, C. Sempoux, F. P. Lemaigre, A. Adili, D. Yuan, A. Weber, K. Unger, M. Heikenwalder, I. A. Leclercq, R. F. Schwabe, Hepatocellular carcinoma originates from hepatocytes and not from the progenitor/biliary compartment. *The Journal of clinical investigation* **125**, 3891-3903 (2015); published online EpubOct 01 (10.1172/JCI77995).
25. K. Tabuchi, G. Chen, T. C. Sudhof, J. Shen, Conditional forebrain inactivation of nicastrin causes progressive memory impairment and age-related neurodegeneration. *J Neurosci* **29**, 7290-7301 (2009); published online EpubJun 03 (10.1523/jneurosci.1320-09.2009).
26. K. Kim, I. J. Goldberg, M. J. Graham, M. Sundaram, E. Bertaggia, S. X. Lee, L. Qiang, R. A. Haeusler, D. Metzger, P. Chambon, Z. Yao, H. N. Ginsberg, U. B. Pajvani, gamma-Secretase Inhibition Lowers Plasma Triglyceride-Rich Lipoproteins by Stabilizing the LDL Receptor. *Cell Metab* **27**, 816-827.e814 (2018); published online EpubApr 3 (10.1016/j.cmet.2018.02.010).
27. Y. Chen, S. Zheng, D. Qi, S. Zheng, J. Guo, S. Zhang, Z. Weng, Inhibition of Notch signaling by a gamma-secretase inhibitor attenuates hepatic fibrosis in rats. *PLoS One* **7**, e46512 (2012)10.1371/journal.pone.0046512).
28. R. Bansal, J. van Baarlen, G. Storm, J. Prakash, The interplay of the Notch signaling in hepatic stellate cells and macrophages determines the fate of liver fibrogenesis. *Sci Rep* **5**, 18272 (2015); published online EpubDec 14 (10.1038/srep18272).
29. F. He, F. C. Guo, Z. Li, H. C. Yu, P. F. Ma, J. L. Zhao, L. Feng, W. N. Li, X. W. Liu, H. Y. Qin, K. F. Dou, H. Han, Myeloid-specific disruption of recombination signal binding protein Jkappa ameliorates hepatic fibrosis by attenuating inflammation through cylindromatosis in mice. *Hepatology* **61**, 303-314 (2015); published online EpubJan (10.1002/hep.27394).
30. L. Hebbard, J. George, Animal models of nonalcoholic fatty liver disease. *Nature reviews. Gastroenterology & hepatology* **8**, 35-44 (2011); published online EpubJan (10.1038/nrgastro.2010.191).
31. M. E. Rinella, R. M. Green, The methionine-choline deficient dietary model of steatohepatitis does not exhibit insulin resistance. *J Hepatol* **40**, 47-51 (2004); published online EpubJan (
32. C. M. Morell, R. Fiorotto, M. Meroni, A. Raizner, B. Torsello, M. Cadamuro, G. Spagnuolo, E. Kaffe, S. Sutti, E. Albano, M. Strazzabosco, Notch signaling and progenitor/ductular reaction in steatohepatitis. *PLoS One* **12**, e0187384 (2017)10.1371/journal.pone.0187384).

33. L. C. Murtaugh, B. Z. Stanger, K. M. Kwan, D. A. Melton, Notch signaling controls multiple steps of pancreatic differentiation. *Proc Natl Acad Sci U S A* **100**, 14920-14925 (2003); published online EpubDec 9 (10.1073/pnas.2436557100).
34. J. J. Pan, M. B. Fallon, Gender and racial differences in nonalcoholic fatty liver disease. *World journal of hepatology* **6**, 274-283 (2014); published online EpubMay 27 (10.4254/wjh.v6.i5.274).
35. M. V. Machado, A. M. Diehl, Pathogenesis of Nonalcoholic Steatohepatitis. *Gastroenterology* **150**, 1769-1777 (2016); published online EpubJun (10.1053/j.gastro.2016.02.066).
36. T. Hardy, F. Oakley, Q. M. Anstee, C. P. Day, Nonalcoholic Fatty Liver Disease: Pathogenesis and Disease Spectrum. *Annual review of pathology* **11**, 451-496 (2016); published online EpubMay 23 (10.1146/annurev-pathol-012615-044224).
37. J. P. Iredale, Hepatic stellate cell behavior during resolution of liver injury. *Seminars in liver disease* **21**, 427-436 (2001); published online EpubAug (10.1055/s-2001-17557).
38. S. L. Friedman, Hepatic stellate cells: protean, multifunctional, and enigmatic cells of the liver. *Physiol Rev* **88**, 125-172 (2008); published online EpubJan (10.1152/physrev.00013.2007).
39. D. Yimlamai, C. Christodoulou, G. G. Galli, K. Yanger, B. Pepe-Mooney, B. Gurung, K. Shrestha, P. Cahan, B. Z. Stanger, F. D. Camargo, Hippo pathway activity influences liver cell fate. *Cell* **157**, 1324-1338 (2014); published online EpubJun 5 (10.1016/j.cell.2014.03.060).
40. X. Wang, A. Lopategi, X. Ge, Y. Lu, N. Kitamura, R. Urtasun, T. M. Leung, M. I. Fiel, N. Nieto, Osteopontin induces ductular reaction contributing to liver fibrosis. *Gut* **63**, 1805-1818 (2014); published online EpubNov (10.1136/gutjnl-2013-306373).
41. M. V. Machado, G. A. Michelotti, T. A. Pereira, G. Xie, R. Premont, H. Cortez-Pinto, A. M. Diehl, Accumulation of duct cells with activated YAP parallels fibrosis progression in non-alcoholic fatty liver disease. *J Hepatol* **63**, 962-970 (2015); published online EpubOct (10.1016/j.jhep.2015.05.031).
42. M. J. Williams, A. D. Clouston, S. J. Forbes, Links between hepatic fibrosis, ductular reaction, and progenitor cell expansion. *Gastroenterology* **146**, 349-356 (2014); published online EpubFeb (10.1053/j.gastro.2013.11.034).
43. M. M. Richardson, J. R. Jonsson, E. E. Powell, E. M. Brunt, B. A. Neuschwander-Tetri, P. S. Bhathal, J. B. Dixon, M. D. Weltman, H. Tilg, A. R. Moschen, D. M. Purdie, A. J. Demetris, A. D. Clouston, Progressive fibrosis in nonalcoholic steatohepatitis: association with altered regeneration and a ductular reaction. *Gastroenterology* **133**, 80-90 (2007); published online EpubJul (10.1053/j.gastro.2007.05.012).
44. I. Mederacke, C. C. Hsu, J. S. Troeger, P. Huebener, X. Mu, D. H. Dapito, J. P. Pradere, R. F. Schwabe, Fate tracing reveals hepatic stellate cells as dominant contributors to liver fibrosis independent of its aetiology. *Nat Commun* **4**, 2823 (2013)10.1038/ncomms3823).
45. W. K. Syn, S. S. Choi, E. Liaskou, G. F. Karaca, K. M. Agboola, Y. H. Oo, Z. Mi, T. A. Pereira, M. Zdanowicz, P. Malladi, Y. Chen, C. Moylan, Y. Jung, S. D. Bhattacharya, V. Teaberry, A. Omenetti, M. F. Abdelmalek, C. D. Guy, D. H. Adams, P. C. Kuo, G. A. Michelotti, P. F. Whitington, A. M. Diehl, Osteopontin is induced by hedgehog pathway activation and promotes fibrosis progression in nonalcoholic steatohepatitis. *Hepatology* **53**, 106-115 (2011); published online EpubJan (10.1002/hep.23998).
46. R. Urtasun, A. Lopategi, J. George, T.-M. Leung, Y. Lu, X. Wang, X. Ge, M. I. Fiel, N. Nieto, Osteopontin, an oxidant stress sensitive cytokine, up-regulates collagen-I via integrin αVβ3 engagement and PI3K/pAkt/NFκB signaling. *Hepatology* **55**, 594-608 (2012)10.1002/hep.24701).
47. J. D. Coombes, M. Swiderska-Syn, L. Dolle, D. Reid, B. Eksteen, L. Claridge, M. A. Briones-Orta, S. Shetty, Y. H. Oo, A. Riva, S. Chokshi, S. Papa, Z. Mi, P. C. Kuo, R. Williams, A. Canbay, D. H. Adams, A. M. Diehl, L. A. van Grunsven, S. S. Choi, W. K. Syn, Osteopontin neutralisation abrogates the liver progenitor cell response and fibrogenesis in mice. *Gut* **64**, 1120-1131 (2015); published online EpubJul (10.1136/gutjnl-2013-306484).
48. A. Sahai, P. Malladi, H. Melin-Aldana, R. M. Green, P. F. Whitington, Upregulation of osteopontin expression is involved in the development of nonalcoholic steatohepatitis in a

dietary murine model. *American journal of physiology. Gastrointestinal and liver physiology* **287**, G264-273 (2004); published online EpubJul (10.1152/ajpgi.00002.2004).
49. Y. Zong, A. Panikkar, J. Xu, A. Antoniou, P. Raynaud, F. Lemaigre, B. Z. Stanger, Notch signaling controls liver development by regulating biliary differentiation. *Development* **136**, 1727-1739 (2009); published online EpubMay (10.1242/dev.029140 dev.029140 [pii]).
50. Q. Shen, S. Christakos, The vitamin D receptor, Runx2, and the Notch signaling pathway cooperate in the transcriptional regulation of osteopontin. *J Biol Chem* **280**, 40589-40598 (2005); published online EpubDec 09 (10.1074/jbc.M504166200).
51. I. Espinoza, L. Miele, Notch inhibitors for cancer treatment. *Pharmacol Ther* **139**, 95-110 (2013); published online EpubAug (10.1016/j.pharmthera.2013.02.003).
52. N. Takebe, D. Nguyen, S. X. Yang, Targeting notch signaling pathway in cancer: clinical development advances and challenges. *Pharmacol Ther* **141**, 140-149 (2014); published online EpubFeb (10.1016/j.pharmthera.2013.09.005).
53. J. H. van Es, M. E. van Gijn, O. Riccio, M. van den Born, M. Vooijs, H. Begthel, M. Cozijnsen, S. Robine, D. J. Winton, F. Radtke, H. Clevers, Notch/gamma-secretase inhibition turns proliferative cells in intestinal crypts and adenomas into goblet cells. *Nature* **435**, 959-963 (2005); published online EpubJun 16 (10.1038/nature03659).
54. D. P. Sparling, J. Yu, K. Kim, C. Zhu, S. Brachs, A. L. Birkenfeld, U. B. Pajvani, Adipocyte-specific blockade of gamma-secretase, but not inhibition of Notch activity, reduces adipose insulin sensitivity. *Mol Metab* **5**, 113-121 (2016); published online EpubFeb (10.1016/j.molmet.2015.11.006).
55. P. Bi, T. Shan, W. Liu, F. Yue, X. Yang, X. R. Liang, J. Wang, J. Li, N. Carlesso, X. Liu, S. Kuang, Inhibition of Notch signaling promotes browning of white adipose tissue and ameliorates obesity. *Nat Med* **20**, 911-918 (2014); published online EpubAug (10.1038/nm.3615).
56. D. Gaudet, D. Brisson, K. Tremblay, V. J. Alexander, W. Singleton, S. G. Hughes, R. S. Geary, B. F. Baker, M. J. Graham, R. M. Crooke, J. L. Witztum, Targeting APOC3 in the familial chylomicronemia syndrome. *The New England journal of medicine* **371**, 2200-2206 (2014); published online EpubDec 4 (10.1056/NEJMoa1400284).
57. M. J. Graham, R. G. Lee, T. A. Bell, 3rd, W. Fu, A. E. Mullick, V. J. Alexander, W. Singleton, N. Viney, R. Geary, J. Su, B. F. Baker, J. Burkey, S. T. Crooke, R. M. Crooke, Antisense oligonucleotide inhibition of apolipoprotein C-III reduces plasma triglycerides in rodents, nonhuman primates, and humans. *Circ Res* **112**, 1479-1490 (2013); published online EpubMay 24 (10.1161/circresaha.111.300367).
58. D. Gaudet, V. J. Alexander, B. F. Baker, D. Brisson, K. Tremblay, W. Singleton, R. S. Geary, S. G. Hughes, N. J. Viney, M. J. Graham, R. M. Crooke, J. L. Witztum, J. D. Brunzell, J. J. Kastelein, Antisense Inhibition of Apolipoprotein C-III in Patients with Hypertriglyceridemia. *The New England journal of medicine* **373**, 438-447 (2015); published online EpubJul 30 (10.1056/NEJMoa1400283).
59. R. S. Geary, D. Norris, R. Yu, C. F. Bennett, Pharmacokinetics, biodistribution and cell uptake of antisense oligonucleotides. *Adv Drug Deliv Rev* **87**, 46-51 (2015); published online EpubJun 29 (10.1016/j.addr.2015.01.008).
60. A. Suzuki, A. M. Diehl, Nonalcoholic Steatohepatitis. *Annual review of medicine* **68**, 85-98 (2017); published online EpubJan 14 (10.1146/annurev-med-051215-031109).
61. M. E. Rinella, Nonalcoholic fatty liver disease: a systematic review. *Jama* **313**, 2263-2273 (2015); published online EpubJun 9 (10.1001/jama.2015.5370).
62. H. Cuervo, C. M. Nielsen, D. A. Simonetto, L. Ferrell, V. H. Shah, R. A. Wang, Endothelial notch signaling is essential to prevent hepatic vascular malformations in mice. *Hepatology* **64**, 1302-1316 (2016); published online EpubOct (10.1002/hep.28713).
63. A. Wittrup, J. Lieberman, Knocking down disease: a progress report on siRNA therapeutics. *Nat Rev Genet* **16**, 543-552 (2015); published online EpubSep (10.1038/nrg3978).
64. C. Lorenzer, M. Dirin, A. M. Winkler, V. Baumann, J. Winkler, Going beyond the liver: progress and challenges of targeted delivery of siRNA therapeutics. *Journal of controlled release : official*

journal of the Controlled Release Society **203**, 1-15 (2015); published online EpubApr 10 (10.1016/j.jconrel.2015.02.003).
65. D. Dehaini, R. H. Fang, L. Zhang, Biomimetic strategies for targeted nanoparticle delivery. *Bioengineering & Translational Medicine* **1**, 30-46 (2016)10.1002/btm2.10004).
66. S. Jors, P. Jeliazkova, M. Ringelhan, J. Thalhammer, S. Durl, J. Ferrer, M. Sander, M. Heikenwalder, R. M. Schmid, J. T. Siveke, F. Geisler, Lineage fate of ductular reactions in liver injury and carcinogenesis. *J Clin Invest* **125**, 2445-2457 (2015); published online EpubJun (10.1172/jci78585).
67. R. M. Mancina, P. Dongiovanni, S. Petta, P. Pingitore, M. Meroni, R. Rametta, J. Boren, T. Montalcini, A. Pujia, O. Wiklund, G. Hindy, R. Spagnuolo, B. M. Motta, R. M. Pipitone, A. Craxi, S. Fargion, V. Nobili, P. Kakela, V. Karja, V. Mannisto, J. Pihlajamaki, D. F. Reilly, J. Castro-Perez, J. Kozlitina, L. Valenti, S. Romeo, The MBOAT7-TMC4 Variant rs641738 Increases Risk of Nonalcoholic Fatty Liver Disease in Individuals of European Descent. *Gastroenterology* **150**, 1219-1230.e1216 (2016); published online EpubMay (10.1053/j.gastro.2016.01.032).
68. C. Postic, M. A. Magnuson, DNA excision in liver by an albumin-Cre transgene occurs progressively with age. *Genesis* **26**, 149-150 (2000); published online EpubFeb (
69. U. B. Pajvani, L. Qiang, T. Kangsamaksin, J. Kitajewski, H. N. Ginsberg, D. Accili, Inhibition of Notch uncouples Akt activation from hepatic lipid accumulation by decreasing mTorc1 stability. *Nat Med* **19**, 1055-+ (2013); published online EpubAug (Doi 10.1038/Nm.3259).
70. C. M. Miller, M. Tanowitz, A. J. Donner, T. P. Prakash, E. E. Swayze, E. N. Harris, P. P. Seth, Receptor-Mediated Uptake of Phosphorothioate Antisense Oligonucleotides in Different Cell Types of the Liver. *Nucleic acid therapeutics* **28**, 119-127 (2018); published online EpubJun (10.1089/nat.2017.0709).
71. L. Lisowski, A. P. Dane, K. Chu, Y. Zhang, S. C. Cunningham, E. M. Wilson, S. Nygaard, M. Grompe, I. E. Alexander, M. A. Kay, Selection and evaluation of clinically relevant AAV variants in a xenograft liver model. *Nature* **506**, 382-386 (2014); published online EpubFeb 20 (10.1038/nature12875).
72. K. Kim, L. Qiang, M. S. Hayden, D. P. Sparling, N. H. Purcell, U. B. Pajvani, mTORC1-independent Raptor prevents hepatic steatosis by stabilizing PHLPP2. *Nat Commun* **7**, 10255 (2016); published online EpubJan 08 (10.1038/ncomms10255).
73. J. Font-Burgada, S. Shalapour, S. Ramaswamy, B. Hsueh, D. Rossell, A. Umemura, K. Taniguchi, H. Nakagawa, M. A. Valasek, L. Ye, J. L. Kopp, M. Sander, H. Carter, K. Deisseroth, I. M. Verma, M. Karin, Hybrid Periportal Hepatocytes Regenerate the Injured Liver without Giving Rise to Cancer. *Cell* **162**, 766-779 (2015); published online EpubAug 13 (10.1016/j.cell.2015.07.026).
74. I. Mederacke, D. H. Dapito, S. Affo, H. Uchinami, R. F. Schwabe, High-yield and high-purity isolation of hepatic stellate cells from normal and fibrotic mouse livers. *Nature protocols* **10**, 305-315 (2015); published online EpubFeb (10.1038/nprot.2015.017).
75. J. Folch, M. Lees, G. H. Sloane Stanley, A simple method for the isolation and purification of total lipides from animal tissues. *The Journal of biological chemistry* **226**, 497-509 (1957); published online EpubMay (
76. J. P. Pradere, J. Kluwe, S. De Minicis, J. J. Jiao, G. Y. Gwak, D. H. Dapito, M. K. Jang, N. D. Guenther, I. Mederacke, R. Friedman, A. C. Dragomir, C. Aloman, R. F. Schwabe, Hepatic macrophages but not dendritic cells contribute to liver fibrosis by promoting the survival of activated hepatic stellate cells in mice. *Hepatology* **58**, 1461-1473 (2013); published online EpubOct (10.1002/hep.26429).

Acknowledgments: We thank A. Flete, T. Kolar and J. Weber for excellent technical support, W. Wang, L. Lu, S. Shah and S. Ho for their assistance with cell sorting, and members of the Pajvani, Tabas, and Schwabe laboratories for insightful discussion. We also gratefully acknowledge J. Clarke and N. Cherrington (Arizona), and N. Tanaka and F. Gonzalez (NIH) for sharing samples related to this work, H. Grajal and J. Kitajewski (UIC) for sharing mouse strains, as well as the Ancillary Studies Committee and Publications and Presentations Committee of the NASH CRN, who reviewed and approved this manuscript.

Funding: Supported by NIH DK103818 (UBP), NIH DK105303 (UBP), MyFIRST AIRC Grant n.16888 (LV), ALF Liver Scholar Award (XW) and an AHA Predoctoral Fellowship 17PRE33120000 (CZ). Cell sorting experiments were performed in the CCTI Flow Cytometry Core, supported by NIH S10OD020056, and the Diabetes and Endocrinology Research Center Flow Core Facility funded in part through NIH 5P30DK063608. The PIVENS trial was supported by NIH U01DK061734 and U01DK061730.

Author contributions: C.Z. designed, performed and interpreted experiments, and wrote the manuscript. K.K., X.W., A.B., M.S., P.D., M.M., K.P.Y., A.M.D, R.F.S., I.T., L.V. and J.E.L performed and interpreted experiments. U.B.P. designed, interpreted experiments and wrote the manuscript.

Competing interests: The authors declare that they have no competing financial interest in the work described.

Data and materials availability: All data associated with this study are present in the manuscript and supplementary materials.

Figures

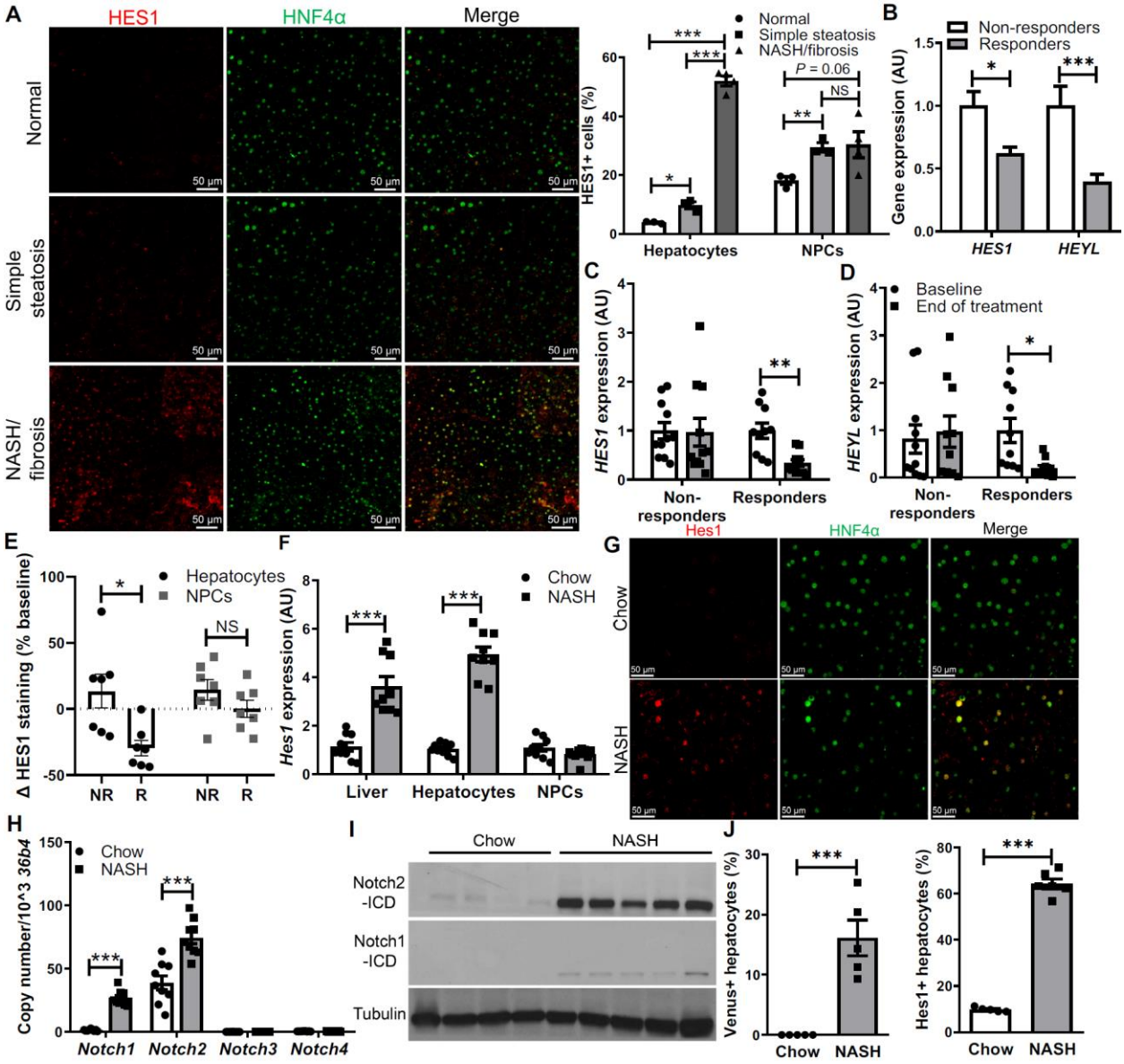

Fig. 1. Hepatocyte Notch activation in NASH. (**A**) Representative images of HES1 (red) and HNF4α (green) immunofluorescence in liver biopsies from patients with histologically normal liver, simple steatosis, or NASH/fibrosis, and quantification of %HES1+ cells among HNF4α+ hepatocytes and HNF4α- non-hepatocytes (n = 3-4/group). (**B**) Expression of Notch target genes *HES1* and *HEYL* after 96 weeks of treatment in Non-responders (n = 49) or Responders (n = 69) from the PIVENS trial. (**C**) Liver *HES1* and (**D**) *HEYL* expression in paired baseline and 96-week end-of-treatment liver biopsy specimens from PIVENS patients (n = 10-11/group), and (**E**) percentage change of HES1+/HNF4α+

hepatocytes and HES1+/HNF4α- nonparenchymal cells (NPCs) in Non-responders (NR) and Responders (R) from baseline to end-of-treatment (n = 7/group). (**F**) *Hes1* expression in liver, fractionated hepatocytes, and NPCs. (**G**) Representative images of Hes1 and HNF4α immunofluorescence in chow and NASH diet-fed WT mouse livers, and quantification of the percentage of hepatocytes with nuclear Hes1 staining (n = 9/group). (**H**) Expression of Notch receptors in hepatocytes and (**I**) western blots of Notch1- and Notch2-intracellular domain (ICD) in livers from chow- and NASH diet-fed WT mice. (**J**) Quantification of Venus+ hepatocytes in livers from chow- and NASH diet-fed Notch reporter mice (n = 5/group). *, $P < 0.05$, **, $P < 0.01$ and ***, $P < 0.001$ as compared to the indicated controls by 2-tailed *t* tests (2 groups) or one-way ANOVA followed by post-hoc *t* tests (3 groups). NS, not significant. Scale bar for all images, 50 μm. AU, arbitrary unit. All data are shown as the means ± s.e.m.

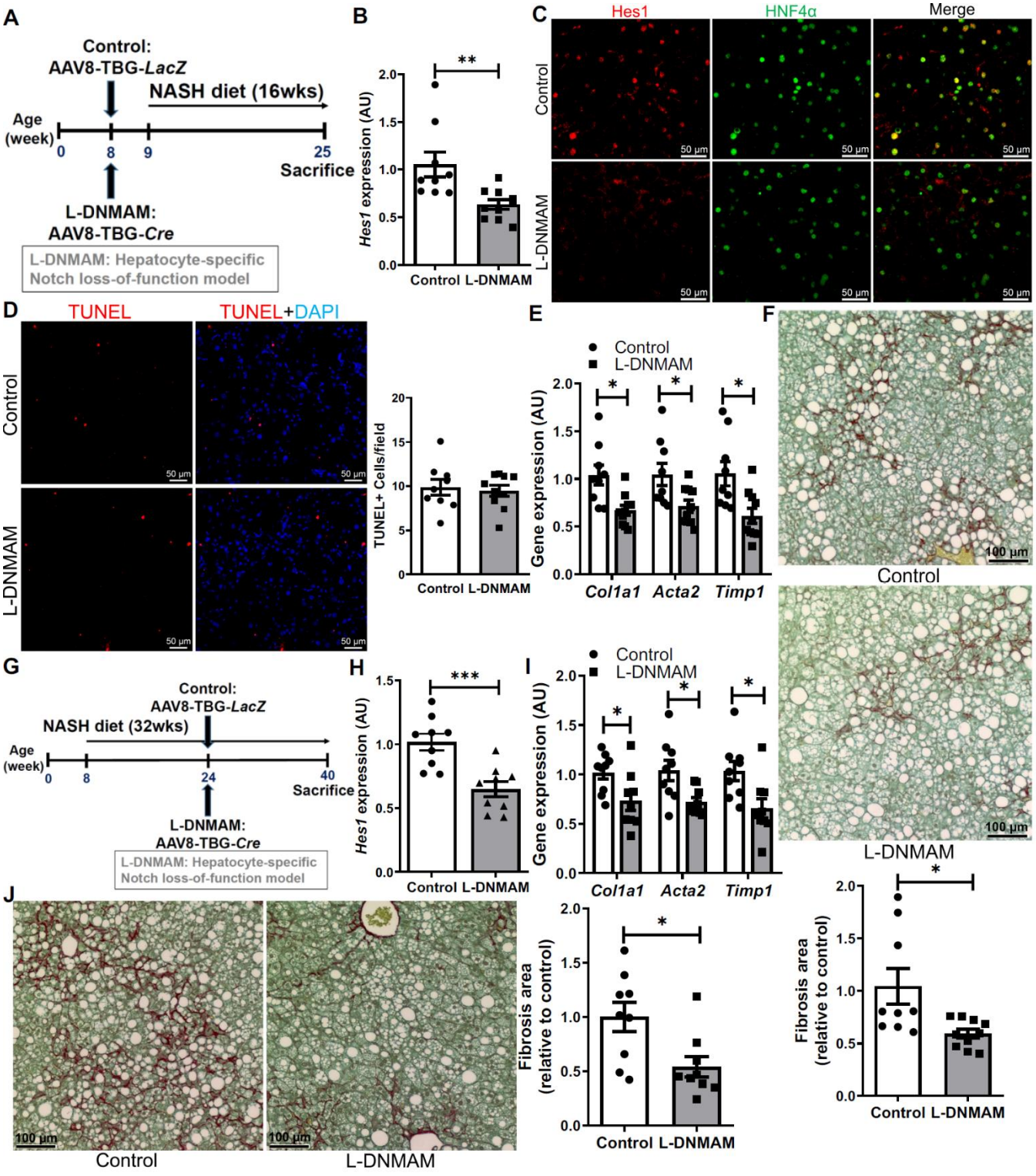

Fig. 2. **Hepatocyte Notch blockade ameliorates NASH-associated fibrosis.** (**A**) 8-week old *Rosa*^{DNMAM} mice were transduced with AAV8-TBG-*LacZ* (Control), or AAV8-TBG-*Cre* to generate hepatocyte-specific dominant-negative MAML-expressing (*L-DNMAM*) mice, then fed for 16 weeks with NASH diet (n = 9-10/group). (**B**) *Hes1* expression, (**C**) representative pictures of Hes1 (red) and HFN4α

(green) staining (scale bar, 50 μm), (**D**) TUNEL (red) staining (scale bar, 50 μm) and quantification, (**E**) expression of fibrogenic genes, and (**F**) liver collagen staining (scale bar, 100 μm) and quantification in livers from Cre- control and *L-DNMAM* mice. (**G**) 8-week old *Rosa*^{DNMAM} mice were fed with NASH diet for 32 weeks with AAV8-TBG-*LacZ* or -*Cre* transduction in the 16th week (n = 9/group). (**H**) *Hes1* and (**I**) fibrogenic gene expression, and (**J**) collagen staining (scale bar, 100 μm) and quantification in livers from Cre- controls and mice with delayed expression of *DNMAM*. *, $P < 0.05$, **, $P < 0.01$ and ***, $P < 0.001$ as compared to the indicated controls by 2-tailed *t* tests (2 groups). AU, arbitrary unit. All data are shown as the means ± s.e.m.

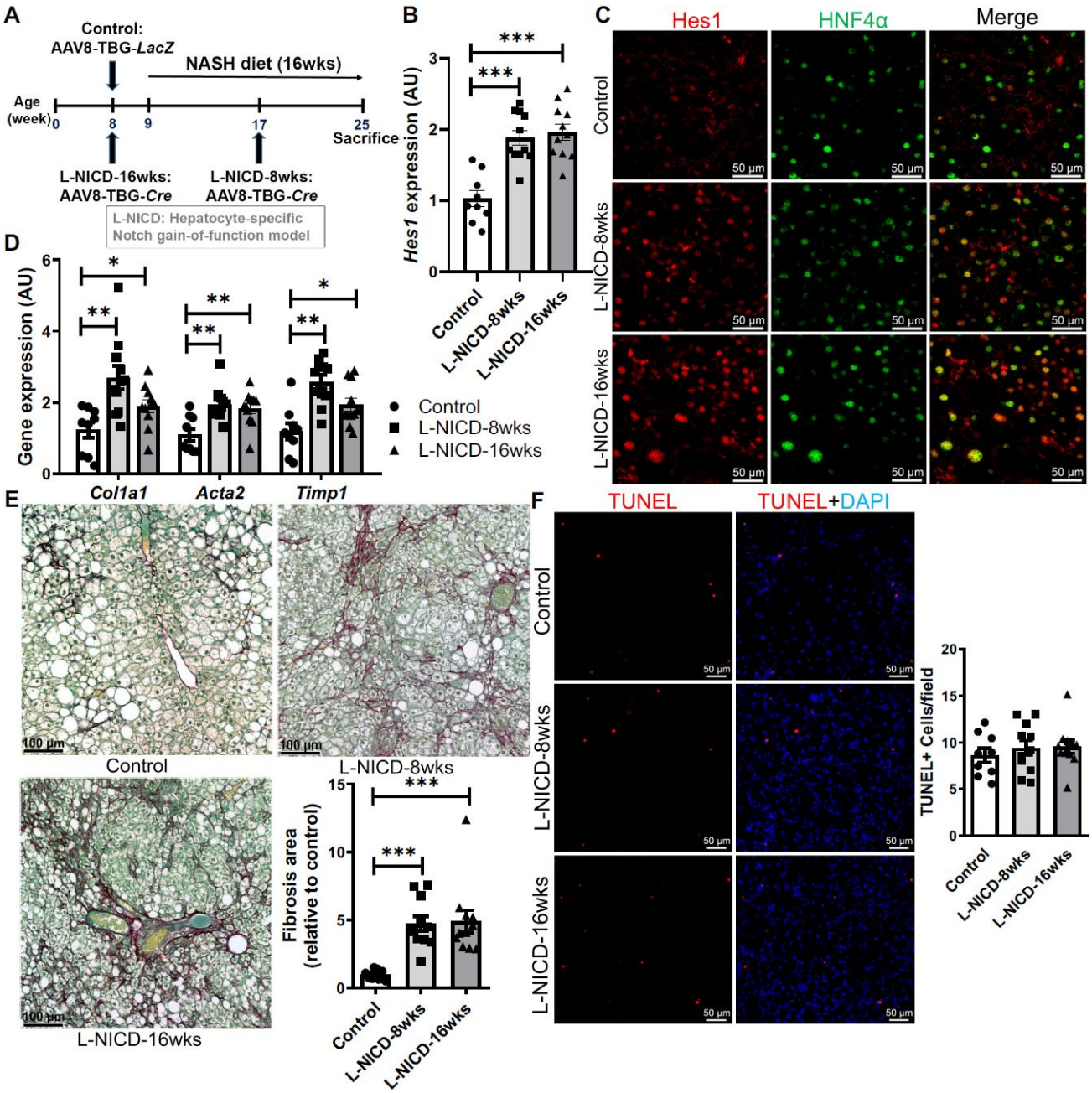

Fig. 3. **Hepatocyte Notch activation exacerbates NASH and fibrosis.** (**A**) 8-week old *Rosa*^{NICD} mice were transduced with AA8V-TBG-*LacZ* (Control), or AAV8-TBG-*Cre* to generate hepatocyte-specific Notch gain-of-function (*L-NICD*-16wks) mice prior to 16 weeks of NASH diet-feeding, or half-way through NASH diet-feeding (*L-NICD*-8wks) (n = 9-11/group). (**B**) *Hes1* expression, (**C**) representative pictures of Hes1 (red) and HFN4α (green) staining (scale bar, 50 μm), (**D**) expression of fibrogenic genes, (**E**) collagen staining (scale bar, 100 μm) and quantification, and (**F**) TUNEL (red) staining (scale bar, 50 μm) in livers from control and *L-NICD* mice. *, $P < 0.05$, **, $P < 0.01$ and ***, $P < 0.001$ as

compared to Cre- control mice by one-way ANOVA followed by post-hoc *t* tests (3 groups). AU, arbitrary unit. All data are shown as the means ± s.e.m.

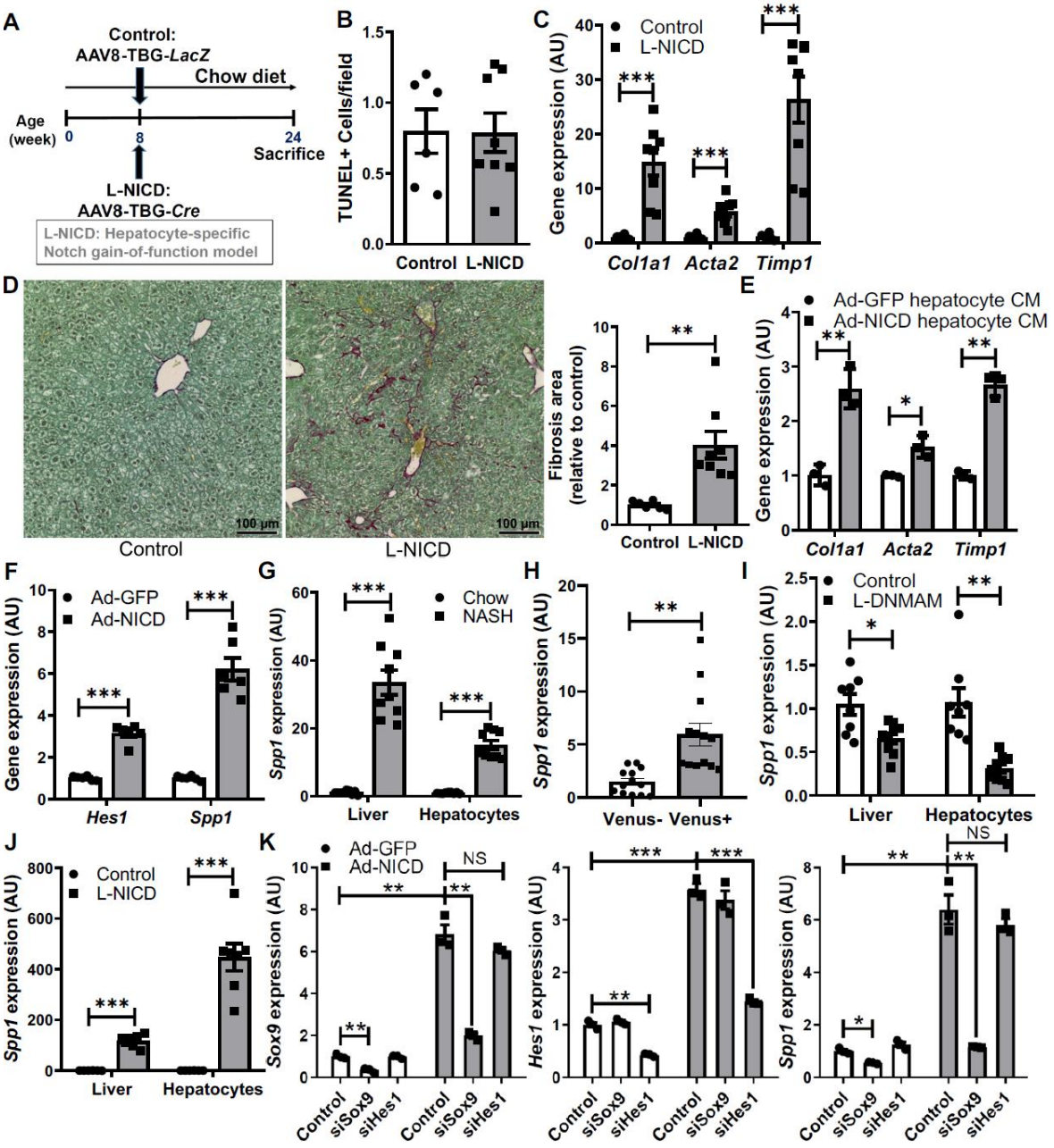

Fig. 4. **Hepatocyte Notch activation in chow-fed mice induces Sox9-dependent *Spp1* expression and liver fibrosis.** (**A**) 8-week old male normal chow-fed *Rosa*^{NICD} mice were transduced with AAV8-TBG-*LacZ* (Control) or AAV-TBG-*Cre* (*L-NICD*) and maintained on normal chow diet for 16 more weeks (n = 68/group). (**B**) Quantification of TUNEL staining, (**C**) fibrogenic gene expression, and (**D**) collagen staining (scale bar, 100 μm) and quantification in livers from control and *L-NICD* mice. (**E**) Fibrogenic

gene expression in plated HSCs isolated form WT mice, exposed to control or Ad-NICD-transduced hepatocyte conditioned medium (CM) (n = 3/group). (**F**) *Hes1* and *Spp1* in control and Notch-activated primary hepatocytes (n = 6/group). (**G** to **J**) *Spp1* expression in (**G**) livers and isolated hepatocytes of NASH diet-fed mice (n = 9/group), (**H**) hepatocytes sorted based on Notch activity from Notch reporter mice (n = 13/group), (**I**) livers and FACS-separated hepatocytes from NASH diet-fed *L-DNMAM* mice (n = 8/group), and (**J**) NASH diet-fed *L-NICD* mice (n = 7/group). (**K**) *Spp1* expression in si*Sox9* or si*Hes1*-transfected primary hepatocytes (n = 3/group). *, $P < 0.05$, **, $P < 0.01$ and ***, $P < 0.001$ as compared to the indicated controls by 2-tailed *t* tests (2 groups) or one-way ANOVA followed by post-hoc *t* tests (more than 2 groups). NS, not significant. AU, arbitrary unit. All data are shown as the means $\pm$ s.e.m.

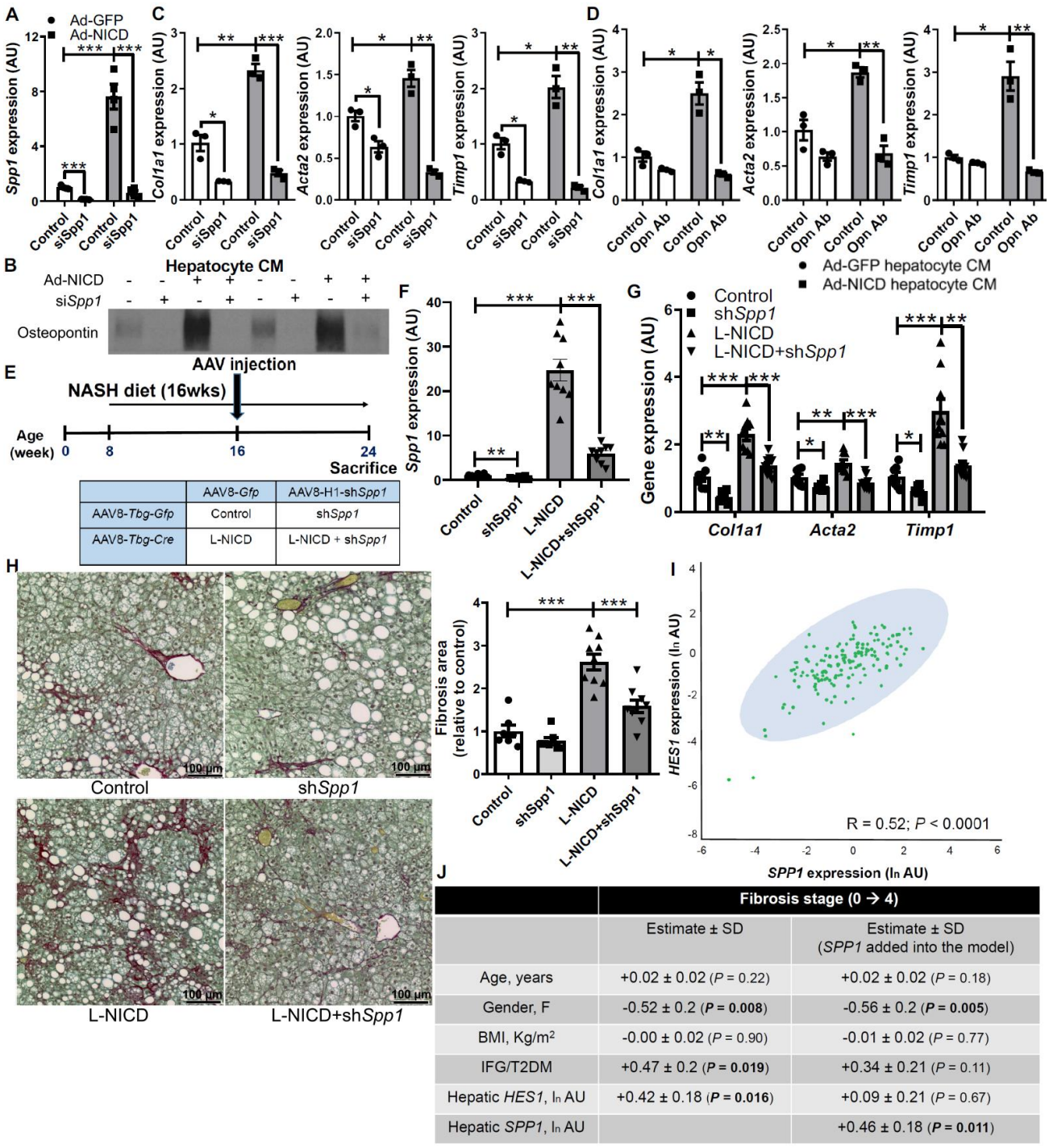

J

	Fibrosis stage (0 → 4)	
	Estimate ± SD	Estimate ± SD (*SPP1* added into the model)
Age, years	+0.02 ± 0.02 (*P* = 0.22)	+0.02 ± 0.02 (*P* = 0.18)
Gender, F	-0.52 ± 0.2 (***P* = 0.008**)	-0.56 ± 0.2 (***P* = 0.005**)
BMI, Kg/m²	-0.00 ± 0.02 (*P* = 0.90)	-0.01 ± 0.02 (*P* = 0.77)
IFG/T2DM	+0.47 ± 0.2 (***P* = 0.019**)	+0.34 ± 0.21 (*P* = 0.11)
Hepatic *HES1*, ln AU	+0.42 ± 0.18 (***P* = 0.016**)	+0.09 ± 0.21 (*P* = 0.67)
Hepatic *SPP1*, ln AU		+0.46 ± 0.18 (***P* = 0.011**)

Fig. 5. **Notch-induced hepatocyte Osteopontin activates HSCs and induces liver fibrosis.**

(**A**) Hepatocyte *Spp1* expression (n = 4/group) and (**B**) Osteopontin secreted in hepatocyte CM from control or Notch-activated hepatocytes transfected with siRNA directed against *Spp1* (si*Spp1*) or scrambled control. Expression of fibrogenic genes in HSCs exposed to CM (**C**) from control or Notch-activated si*Spp1*-transfected hepatocytes (n = 3/group), or (**D**) CM pre-treated with an Osteopontin

neutralizing antibody (n = 3/group). (**E**) 8-week old *Rosa*^{NICD} mice were fed with NASH diet for 8 weeks, then transduced with AAV8-TBG-*Gfp* or AAV8-TBG-*Cre* (to generate Control and *L-NICD* mice) and simultaneously with AAV8-H1-*Gfp* or AAV8-H1-sh*Spp1* (n = 7-9/group). (**F**) *Spp1* and (**G**) fibrogenic gene expression, and (**H**) collagen staining (scale bar, 100 μm) and quantification in livers from control and *L-NICD* mice transduced with sh*Spp1*. *, $P < 0.05$, **, $P < 0.01$ and ***, $P < 0.001$ as compared to the indicated controls by one-way ANOVA followed by post-hoc *t* tests (more than 2 groups). All data are shown as the means ± s.e.m. (**I**) Correlation between *HES1* and *SPP1* expression in liver biopsies from patients at risk of NASH (n = 159). (**J**) Table of association between *HES1* expression and liver fibrosis stage, after adjustment for key demographic variables (left column) or when additionally adjusted for *SPP1* expression (right column). Expression of *HES1* and *SPP1* were log transformed to ensure the assumption of normal distribution. All data in the table are shown as the regression estimates ± SD and *P*-values, which were generated by multivariate ordinal regression analyses. AU, arbitrary unit.

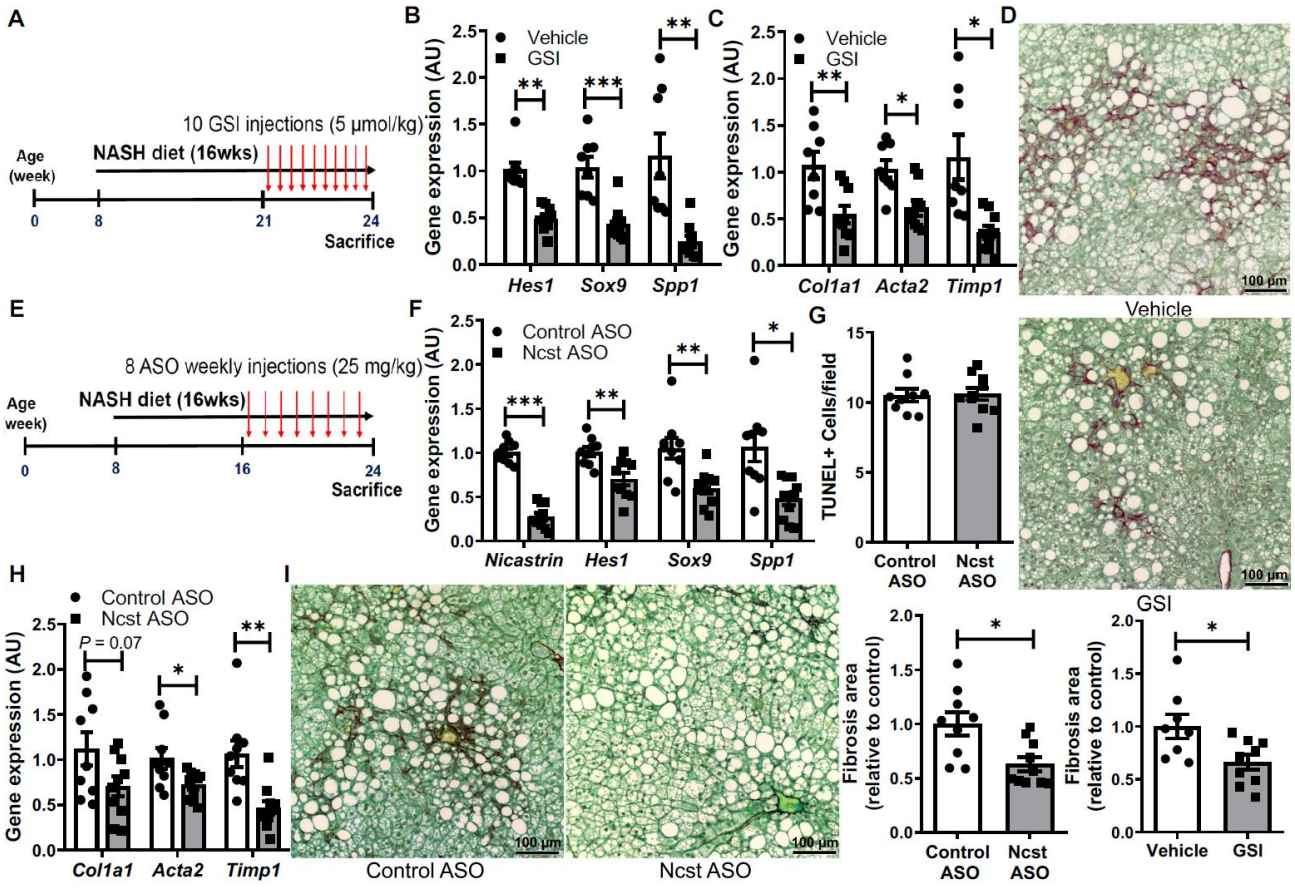

Fig. 6. **Pharmacologic Notch inhibitors ameliorate NASH diet-induced fibrosis**. (**A**) WT mice received vehicle or GSI (5 µmol/kg body weight) every other day for the last 3 weeks of NASH diet-feeding (n = 8-9/group). (**B**) Expression of Notch targets and (**C**) fibrogenic genes, and (**D**) collagen staining (scale bar, 100 µm) and quantification in livers from vehicle or GSI-treated mice. (**E**) WT mice received weekly injections of control or *Nicastrin* (*Ncst*) ASO (25 mg/kg) for the last 8 weeks of NASH diet-feeding (n = 9-10/group). (**F**) *Nicastrin* and Notch target gene expression, (**G**) quantification of TUNEL staining, (**H**) expression of fibrogenic genes, and (**I**) collagen staining (scale bar, 100 µm) and quantification in livers from control or *Ncst* ASO-treated mice. *, $P < 0.05$, **, $P < 0.01$ and ***, $P < 0.001$ as compared to the indicated controls by 2-tailed *t* tests (2 groups). AU, arbitrary unit. All data are shown as the means ± s.e.m.

Supplementary Materials

Supplementary Materials and Methods

γ-secretase inhibitor (GSI) and Antisense oligonucleotide (ASO) studies. GSI was used as previously described (*15, 54, 69*). In short, DBZ (Syncom) was suspended in vehicle [0.5% Methocel E4M (wt/vol, Colorcon) and 0.1% (vol/vol) Tween-80 (Sigma)]. Immediately prior to injection, DBZ was sonicated for 2 minutes to suspension, and administered once daily by intraperitoneal injection to male C57BL/6J mice for 7 days at 10 μmol/kg body weight, or every other day for 20 days at 5 μmol/kg body weight. Control ASO (GGCCAATACGCCGTCA) and *Nicastrin* ASO (CAGAATAGACTTCCTC) were synthesized by Ionis Pharmaceuticals (*26*). Single strand ASOs do not require expients, with uptake facilitated by both passive diffusion and receptor-mediated endocytic mechanisms (*70*). Both ASOs were dissolved in saline and administered by intraperitoneal injection to male C57BL/6J mice at a dose of 25 mg/kg body weight once weekly for 8 weeks prior to sacrifice.

AAV and adenovirus experiments. Adeno-associated virus subtype 8 (AAV8) containing hepatocyte-specific *Cre* recombinase (AAV-TBG-*Cre*, AV-8-PV1091) and control vector (AAV-TBG-*LacZ*, AV-8-PV0142) were obtained from the Penn Vector Core and administered to 8-week-old $Rosa^{DNMAM}$ and $Rosa^{NICD}$ mice by tail vein injection at a dose of 1.5×10^{11} genome copies/mouse, 1 week prior to initiation of NASH diet, unless otherwise noted. AAV8-shRNA targeting mouse *Spp1* was made by annealing complementary oligonucleotides (5'-CACCACTCTTAGCTTAGTCTGTTGTTTCAAGA GAACAACAGACTAAGCTAAGAG-3'), which were ligated into the self-complementary AAV8-RSV-GFP-H1 vector (*71*). The final construct AAV8-H1-sh*Spp1* was amplified by the Salk Institute Gene Transfer, Targeting, and Therapeutics Core. Ad-NICD and Ad-GFP adenoviruses have been described (*69*). We transduced primary hepatocytes at a multiplicity of infection (MOI) of 10 to achieve 90–100% infection efficiency as assessed by GFP+ hepatocytes.

Cell isolation. Hepatocytes were isolated as previously described (*72*). In brief, mice were anaesthetized with ketamine/xylazine (Sigma) and inferior vena cava cannulated with a 22-gauge

catheter (Terumo Medical). After transection of the portal vein, EGTA-containing perfusion buffer was infused followed by a type I collagenase solution (Worthington Biochemical). After collagenase digestion, the liver was removed, minced and further digested in pronase solution to release NPCs. Individual cells were filtered through a 100 μm cell strainer then 50 g centrifugation to separate pelleted hepatocytes, which was further purified by Percoll gradient, and NPC-containing supernatant that was subsequently pelleted by 580 g centrifugation and subjected to 14.5% Nycodenz gradient for further purification. In some experiments, including isolation of hepatocytes from NASH diet-fed WT, *L-DNMAM*, *L-NICD* and Notch-Venus reporter mice, hepatocytes were purified by cell size (FSC) and granularity (SSC) as described (*73*). Total NPCs were further fractionated by FACS to HSCs (via Vitamin A fluorescence (*74*)) and liver myeloid cells [with CD45-APC (BD Biosciences, #559864) and CD11b-FITC (BD Biosciences, #553310)].

Quantitative reverse-transcription PCR. RNA was extracted from liver with Trizol (ThermoFisher) or isolated cells with NucleoSpin RNA (Clontech), prior to cDNA synthesis (ThermoFisher) and quantitative PCR with a DNA Engine Opticon 2 System (Bio-Rad) and Power SYBR Green (ThermoFisher). mRNA expression was normalized to housekeeping genes using the ΔΔC(t) method and presented as relative transcript expression (arbitrary unit). For mouse mRNAs, the expression was normalized to *Tbp*. Absolute mRNA copy numbers were determined for each Notch receptor using primer-specific standard curves, then normalized to *36b4*, and presented as relative transcript levels (copy number/10^3 *36b4*). For human mRNAs, the expression was normalized to either *18S* (PIVENS) or *ACTB* (cross-sectional analysis). Primer sequences are listed in table S3.

Serum transaminase measurement. Serum ALT (Teco Diagnostics) and AST (ThermoFisher, TR70121) were measured and analyzed according to the manufacturer's instructions.

Hepatic lipid measurement. Liver lipids were extracted by the Folch method (*75*), and hepatic triglyceride (Thermo) and Cholesterol E (Wako) measured using colorimetric assays based on the manufacturers' protocols.

Immunohistochemistry and quantification. Following sacrifice and rapid excision of the liver, tissues were fixed in 4% paraformaldehyde at 4 ºC for 24 hours and later embedded in paraffin, sectioned into 5 µm thickness slides which were deparaffinized, rehydrated and stained for immunohistochemical analysis, including H&E, PAS and Sirius red staining. A minimum of 15 low-power fields of Sirius red images per mouse were taken using a polarized light filter and analyzed by Adobe Photoshop as previously described (*76*). PAS staining quantification was done by taking 5-8 non-overlapping pictures in randomly chosen fields per mouse intestinal section from at least 5 animals per experiment, then directly counting staining-positive cells. Images for quantification and representative pictures were taken with a Zeiss light microscope coupled with an AxioCam camera (MR3; Carl Zeiss).

Immunofluorescence and quantification. For immunostaining of human liver biopsies, paraffinized slides were deparaffinized and rehydrated as previously described (*16*), prior to antigen retrieval by incubating slides in HistoVT One (Nacalai) in a 100 ºC steam cooker for 20 minutes. Slides were then incubated at 4 ºC overnight with primary antibodies against HES1 (Santa Cruz, sc-25392, 1:100), HNF4α (Santa Cruz, sc-6556, 1:100), aSMA (DAKO, M085101-2, 1:300) and CK7 (DAKO, M701801-2, 1:300), then secondary antibodies (anti-mouse Alexa Fluor 488, Invitrogen, A-21202, 1:500; anti-rabbit Alexa Fluor 555, Invitrogen, A-31572, 1:500; donkey anti-goat Alexa Fluor 647, Invitrogen, A-21447, 1:500) prior to mounting with SlowFade Diamond Antifade DAPI Mountant (ThermoFisher, S36973).

For immunostaining of mouse livers, after harvest, tissues were fixed in 4% paraformaldehyde, followed by incubation in 30% sucrose overnight for cryopreservation. Tissues were embedded

with OCT (Tissue Tek), stored at -80 °C, then slides prepared with 7 µM thickness sectioned. Antigen retrieval was performed by incubating frozen slides in HistoVT One solution (Nacalai) in a 70 ºC water bath for 20 minutes. Slides were incubated at 4 ºC overnight with primary antibodies against Hes1 (Santa Cruz, sc-25392, 1:100), HNF4α (Santa Cruz, sc-6556, 1:100), CD45 (BD Biosciences, 550539, 1:100), GFP (Abcam, ab6673, 1:200), CK19 (Abcam, ab52625, 1:300), Osteopontin (R&D Systems, AF808, 1:200) and Alexa Fluor 488-, 555- and 647-conjugated secondary antibodies (Invitrogen). TUNEL staining was performed by using the in situ cell death detection kit (Sigma, #12156792910) based on the manufacturer's protocol.

For quantification, pictures of 15 to 20 non-overlapping and randomly chosen fields per section were taken from at least 5 animals per experiment with a Zeiss Confocal microscope (Axio Observer Z1 with LSM 710 scanning module). Quantification was performed by directly counting staining-positive cells on ZEN 2 software; for nuclear antigens (HES1 and HNF4α), only cells with a clear nuclear staining pattern were counted.

Western Blotting. Liver tissues were lysed in a Triton-based lysis buffer and whole-cell lysates obtained by subsequent centrifugation. Lysate, or hepatocyte conditioned media (CM) was mixed with SDS sample buffer prior to SDS-PAGE. Immunoblots were conducted as previously described (*72*) with primary antibodies against Notch1 (Cell signaling, 4380, 1:1000), Notch2 (Cell signaling, 5732, 1:1000), α-Tubulin (Sigma, T5168, 1:3000), β-Actin (Cell signaling, 4970, 1:2000) and Osteopontin (R&D Systems, AF808, 1:2000).

siRNA and neutralizing antibody *in vitro* experiments. siRNA against mouse *Spp1* (GAAGAUGAUAGGUAUCUGAAAUUCC), *Sox9* (CUACUCCACCUUCACUUACAUGAAC), *Hes1* (CUCUUCUGACGGACACUAAAAACGA) and scrambled control (CGUUAAUCGCGUAUAAUACGCGUAT) were purchased from Integrated DNA Technologies, and transfected into primary hepatocytes derived from 8-week-old C57BL/6J mice using Lipofectamine 300

(ThermoFisher, #L3000015) according to the manufacturer's instructions, with simultaneous Ad-GFP or Ad-NICD adenoviral transduction. In some experiments, transfected hepatocytes were cultured in serum-free DMEM for 24 hours for CM collection. In parallel, HSCs from other 8-week-old C57BL/6J mice were isolated as described (*74*) and serum-starved overnight before CM incubation. Alternatively, Osteopontin neutralizing antibody (R&D Systems, AF808) was added directly into the CM at the recommended ND_{50} of 1 µg/mL prior to HSC incubation.

Cytokine array. 100 µl CM from Ad-GFP or Ad-NICD-transduced (n=3 wells/sample) primary hepatocytes isolated from WT mice were pooled, then applied to a Proteome Profiler Mouse XL Cytokine Array kit (R&D Systems, ARY028) to survey 111 different secreted cytokines. Each cytokine has technical duplicates as well as two biological replicates. Array signals were analyzed using ImageJ (NIH), and the average pixel density used to compare differences between groups.

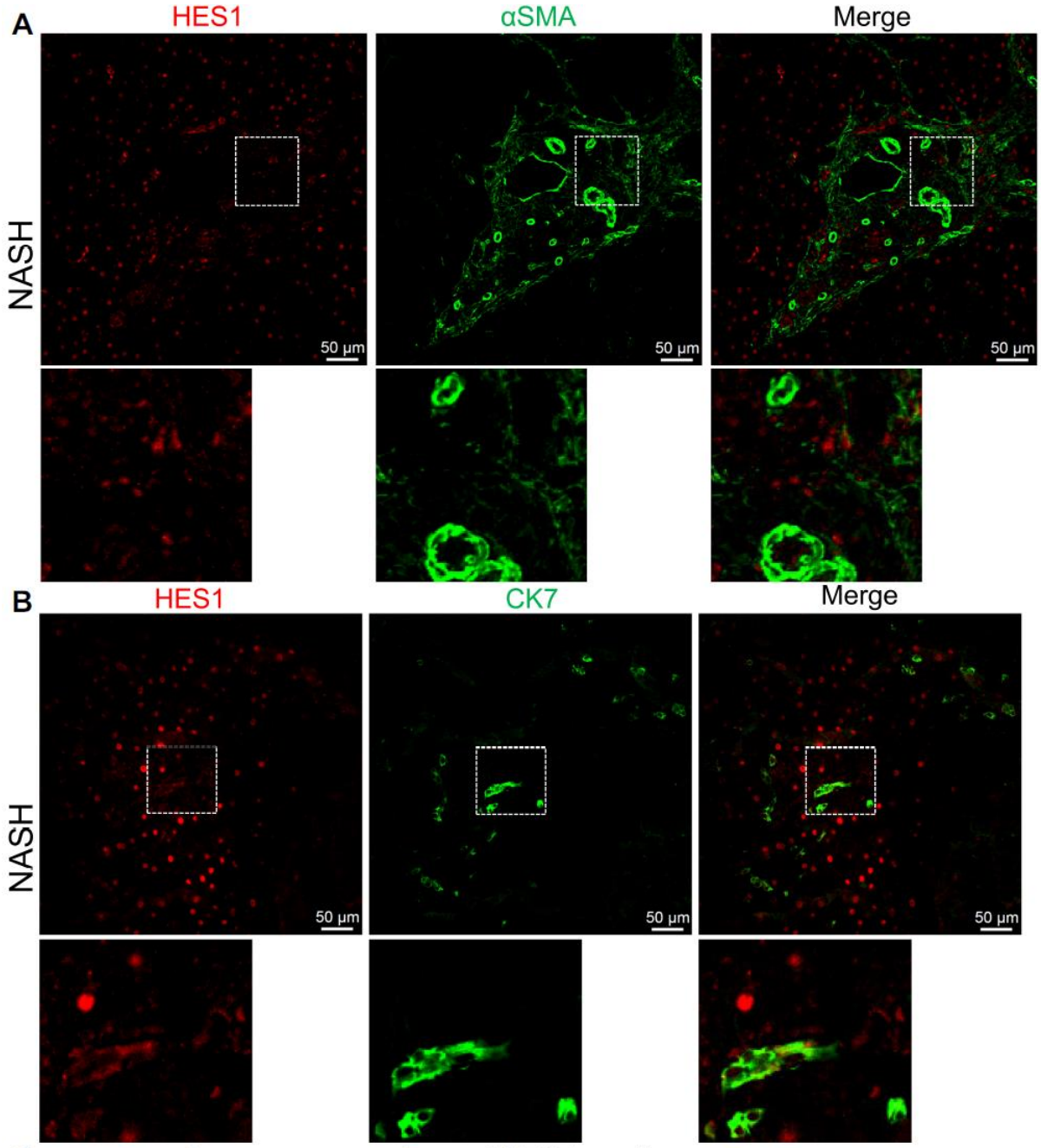

C

Average percentage of HES1+ cells

Cell type	Normal	SS	NASH
Hepatocytes (HNF4α+)	4%	10%	52%
Myofibroblasts (αSMA+)	35%	35%	30%
Cholangiocytes (CK7+)	65%	70%	80%

Fig. S1. HES1 in αSMA+ myofibroblasts and CK7+ cholangiocytes in human livers. (**A**) Representative images of HES1 (red) colocalization with αSMA (green)-positive myofibroblasts or (**B**) CK7 (green)-positive cholangiocytes in liver biopsies from patients with NASH. Scale bar, 50 μm. (**C**) Quantitation of %HES1+ cells in histologically normal livers, livers with simple steatosis (SS) or NASH (n = 3/group).

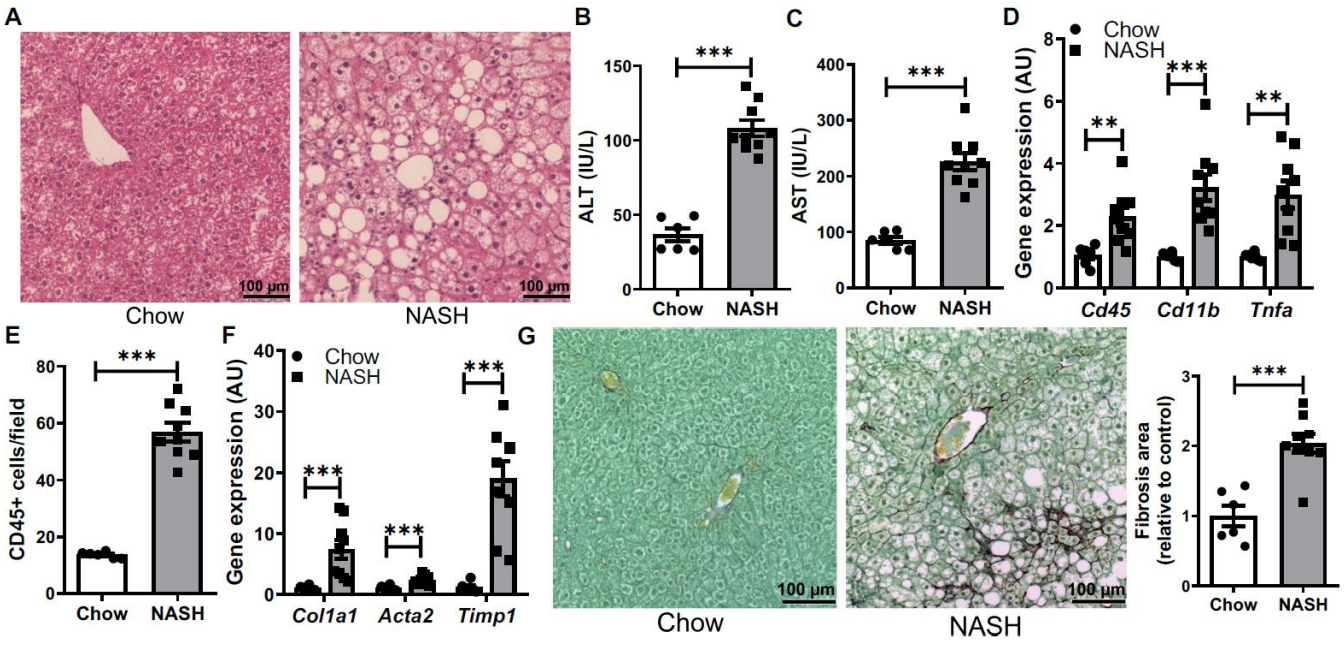

Fig. S2. NASH diet-feeding induces steatohepatitis and fibrosis in WT mice. (**A**) Liver H+E staining, (**B**) serum ALT and (**C**) AST, (**D**) liver inflammatory gene expression, (**E**) CD45+ cell infiltration, (**F**) fibrogenic gene expression and (**G**) collagen deposition in WT mice fed normal chow or NASH diet for 16 weeks (n = 6/group). **, $P < 0.01$ and ***, $P < 0.001$ as compared to chow-fed control WT mice by 2-tailed *t* tests (2 groups). Scale bar for all images, 100 μm. AU, arbitrary unit. All data are shown as the means ± s.e.m.

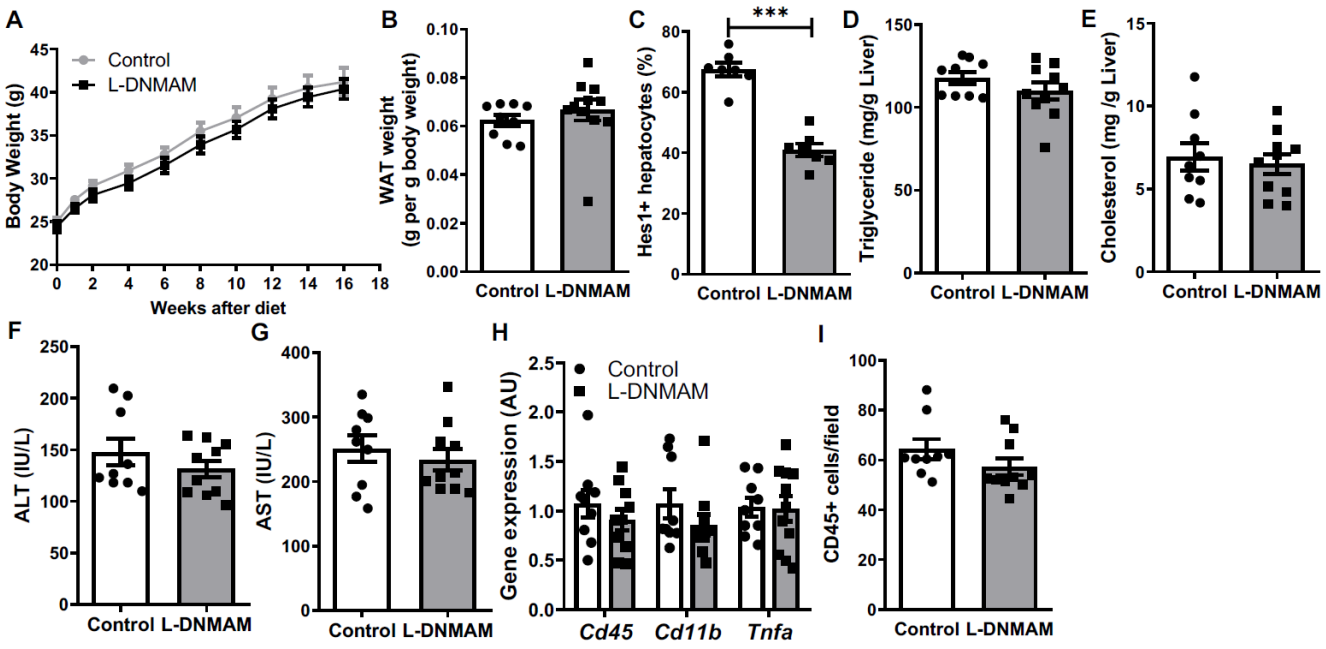

Fig. S3. Characterization of NASH diet-fed *L-DNMAM* mice. (**A**) Body weight curve, (**B**) epididymal white adipose tissue (WAT) weight, (**C**) staining quantification of Hes1+ hepatocytes (related to **Fig. 2C**), (**D**) liver triglyceride and (**E**) cholesterol, (**F**) serum ALT and (**G**) AST, (**H**) liver inflammatory gene expression and (**I**) hepatic CD45+ cell infiltrate in Cre- controls and *L-DNMAM* mice fed NASH diet for 16 weeks (n = 9-10/group). ***, $P < 0.001$ as compared to Cre- controls by 2-tailed *t* tests (2 groups). AU, arbitrary unit. All data are shown as the means ± s.e.m.

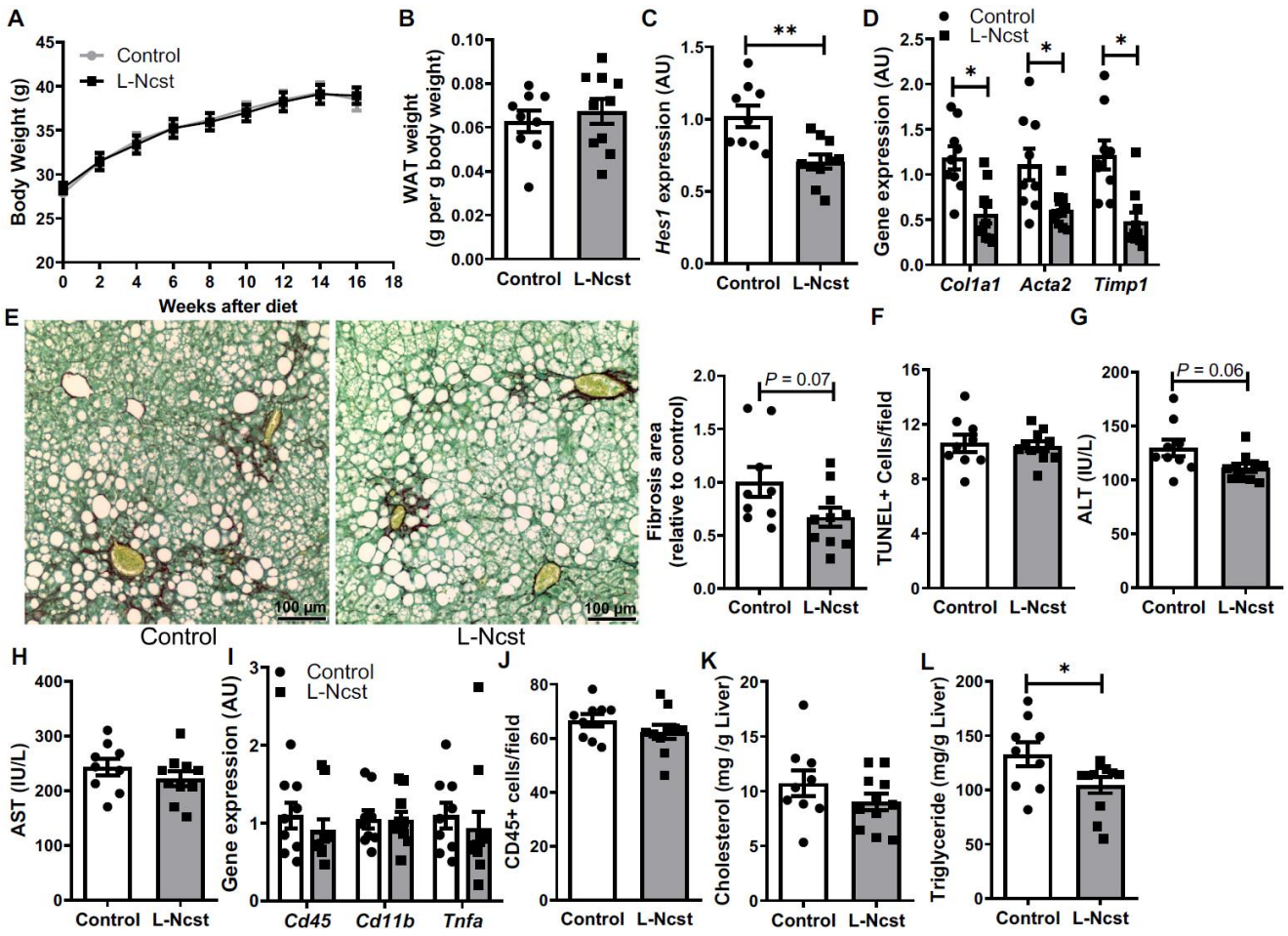

Fig. S4. **Characterization of NASH diet-fed *L-Ncst* mice.** (**A**) Body weight curve, (**B**) epididymal WAT weight, (**C**) liver *Hes1* and (**D**) fibrogenic gene expression, (**E**) liver collagen deposition (scale bar, 100 μm), (**F**) staining quantification of liver TUNEL+ cells, (**G**) serum ALT and (**H**) AST, (**I**) liver inflammatory gene expression, (**J**) CD45+ cell infiltrate, (**K**) cholesterol and (**L**) triglyceride in Cre- and *L-Ncst* mice fed NASH diet for 16 weeks (n = 9-10/group). *, $P < 0.05$ as compared to Cre- controls by 2-tailed *t* tests (2 groups). AU, arbitrary unit. All data are shown as the means ± s.e.m.

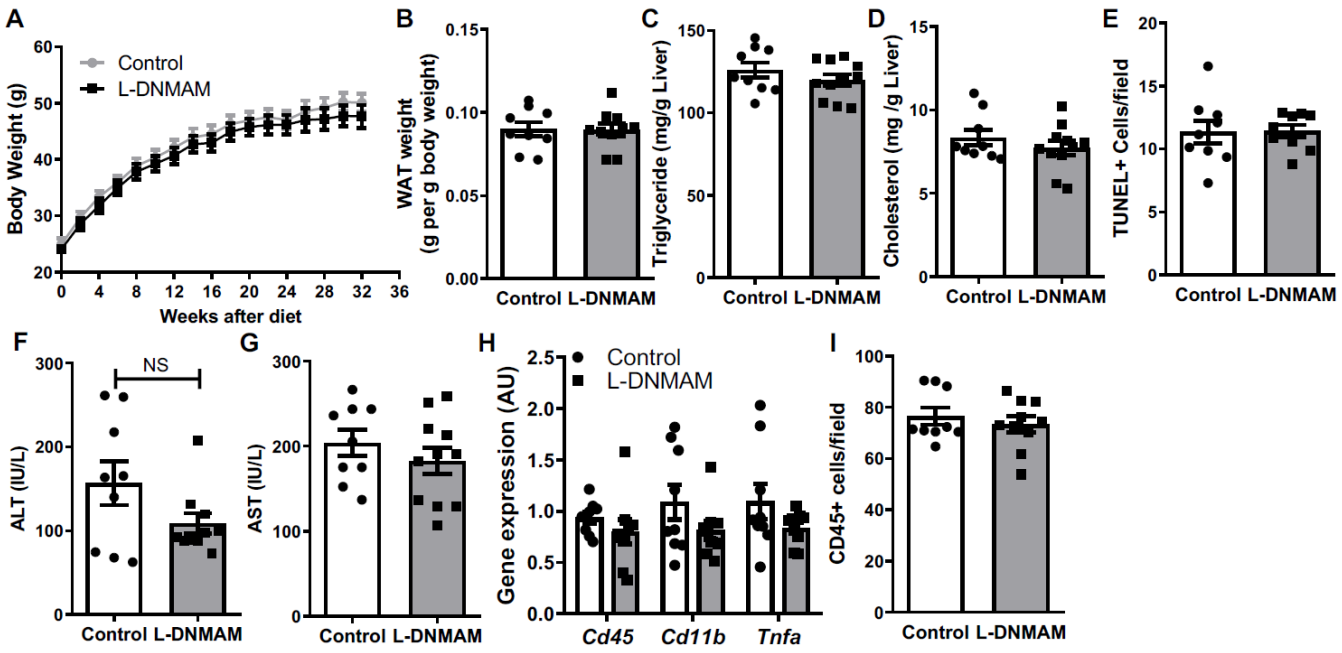

Fig. S5. Characterization of *L-DNMAM* mice on NASH diet for 32 weeks. (**A**) Body weight curve, (**B**) epididymal WAT weight, (**C**) liver triglyceride and (**D**) cholesterol, (**E**) quantification of liver TUNEL+ cells, (**F**) serum ALT and (**G**) AST, (**H**) liver inflammatory gene expression and (**I**) CD45+ cell infiltrate in Cre- controls and *L-DNMAM* mice with Cre-mediated recombination induced 16 weeks after NASH diet initiation (n = 9/group). 2-tailed *t* tests were performed to compare the two groups. NS, not significant. AU, arbitrary unit. All data are shown as the means ± s.e.m.

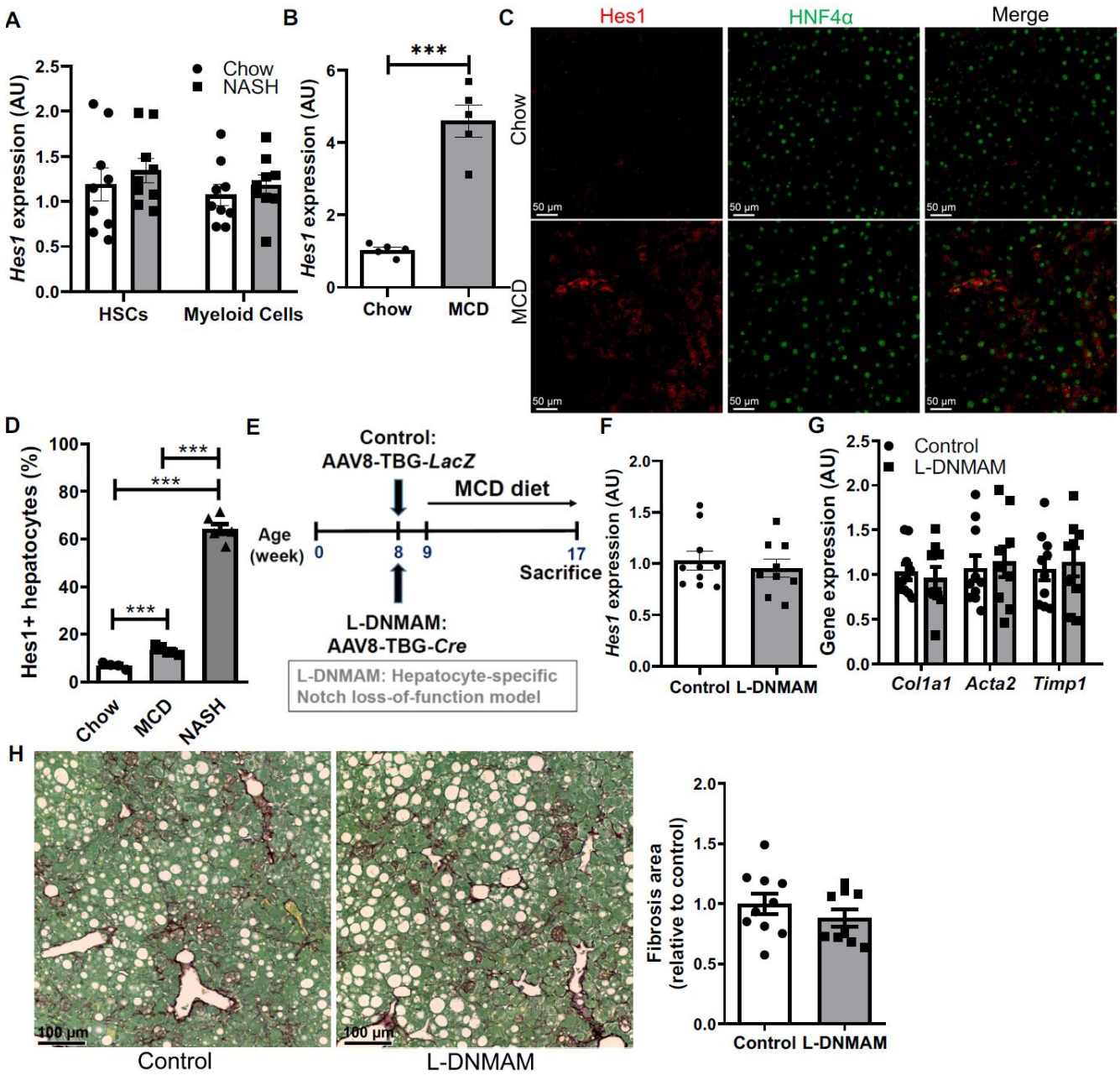

Fig. S6. **Hepatocyte Notch loss-of-function does not protect from MCD-induced liver fibrosis.** (**A**) *Hes1* expression in FACS-sorted HSCs (hepatic stellate cells) and myeloid cells from chow and NASH diet-fed WT mice (n = 9/group). (**B**) Liver *Hes1* expression and (**C**) representative images of Hes1 and HNF4α immunofluorescence in chow and MCD diet-fed mice (scale bar, 50 μm), with (**D**) quantification of nuclear Hes1+ hepatocytes relative to NASH diet-fed mice (n = 5/group). (**E**) 8-week old *Rosa*^{DNMAM} male mice were transduced with AAV8-TBG-*LacZ* (Control) or AAV8-TBG-*Cre* (*L-DNMAM*) prior to 8 weeks of MCD diet-feeding (n = 9-10/group). (**F**) Liver *Hes1*, (**G**) fibrogenic gene

expression and (**H**) collagen deposition (scale bar, 100 μm) in MCD-fed Cre- and *L-DNMAM* mice. **, $P < 0.01$ and ***, $P < 0.001$ as compared to the indicated controls by 2-tailed *t* tests (2 groups) or one-way ANOVA followed by post-hoc *t* tests (3 groups). AU, arbitrary unit. All data are shown as the means ± s.e.m.

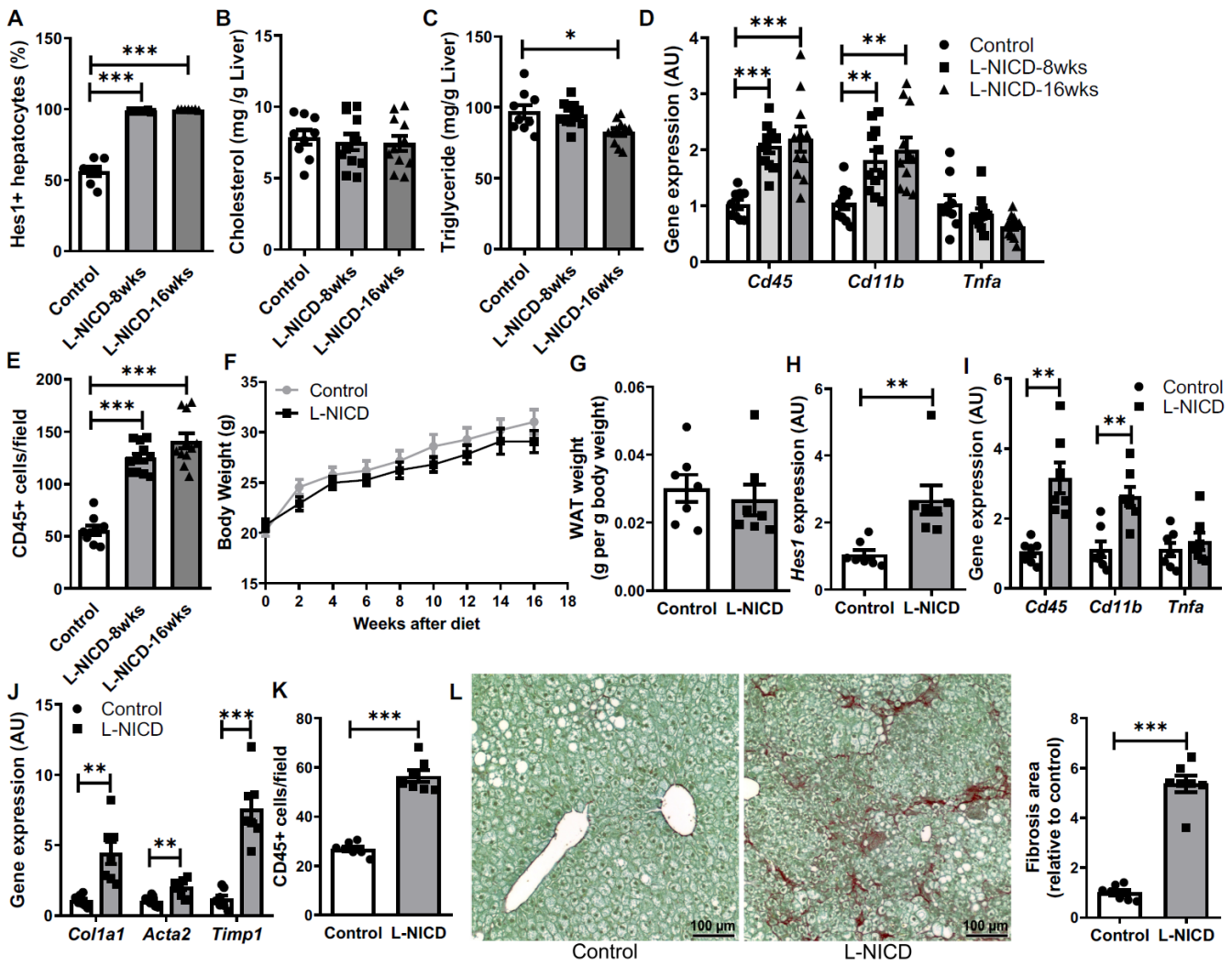

Fig. S7. Characterization of NASH diet-fed Notch gain-of-function mice. (**A**) Quantification of Hes1+ hepatocytes (related to **Fig. 3C**), (**B**) liver cholesterol, (**C**) triglyceride, (**D**) inflammatory gene expression and (**E**) CD45+ cell infiltrate in Cre- and *L-NICD* male mice fed NASH diet for 16 weeks (n = 9-11/group). (**F**) Body weight curve, (**G**) epididymal WAT weight, (**H**) liver *Hes1*, (**I**) inflammatory and (**J**) fibrogenic gene expression, (**K**) CD45+ infiltrate and (**L**) collagen deposition (scale bar, 100 μm) in Cre- and *L-NICD* female mice fed NASH diet for 16 weeks (n = 7/group). *, $P < 0.05$, **, $P < 0.01$ and ***, $P < 0.001$ as compared to Cre- controls by 2-tailed *t* tests (2 groups) or one-way ANOVA followed by post-hoc *t* tests (3 groups). AU, arbitrary unit. All data are shown as the means ± s.e.m.

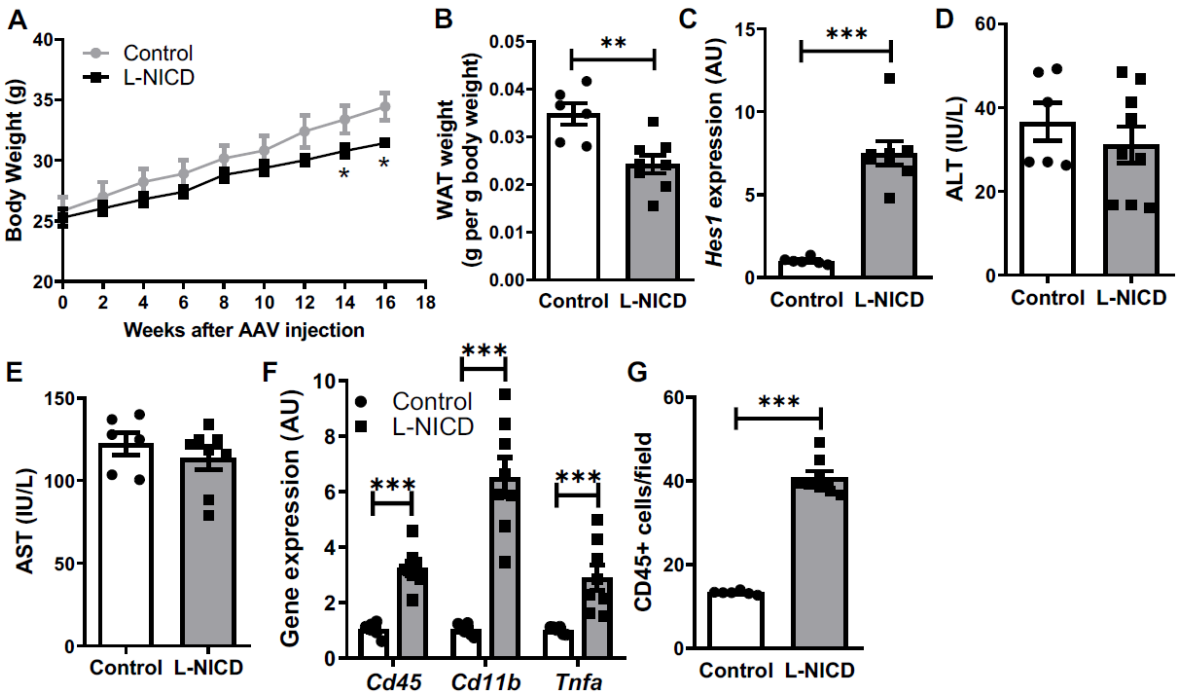

Fig. S8. **Characterization of chow-fed *L-NICD* male mice.** (**A**) Body weight curve, (**B**) epididymal WAT weight, (**C**) liver *Hes1*, (**D**) serum ALT and (**E**) AST, (**F**) liver inflammatory gene expression and (**G**) CD45+ cell infiltrate in chow-fed Cre- and *L-NICD* male mice (n = 6-8/group). **, $P < 0.01$ and ***, $P < 0.001$ as compared to Cre- controls by 2-tailed *t* tests (2 groups). AU, arbitrary unit. All data are shown as the means ± s.e.m.

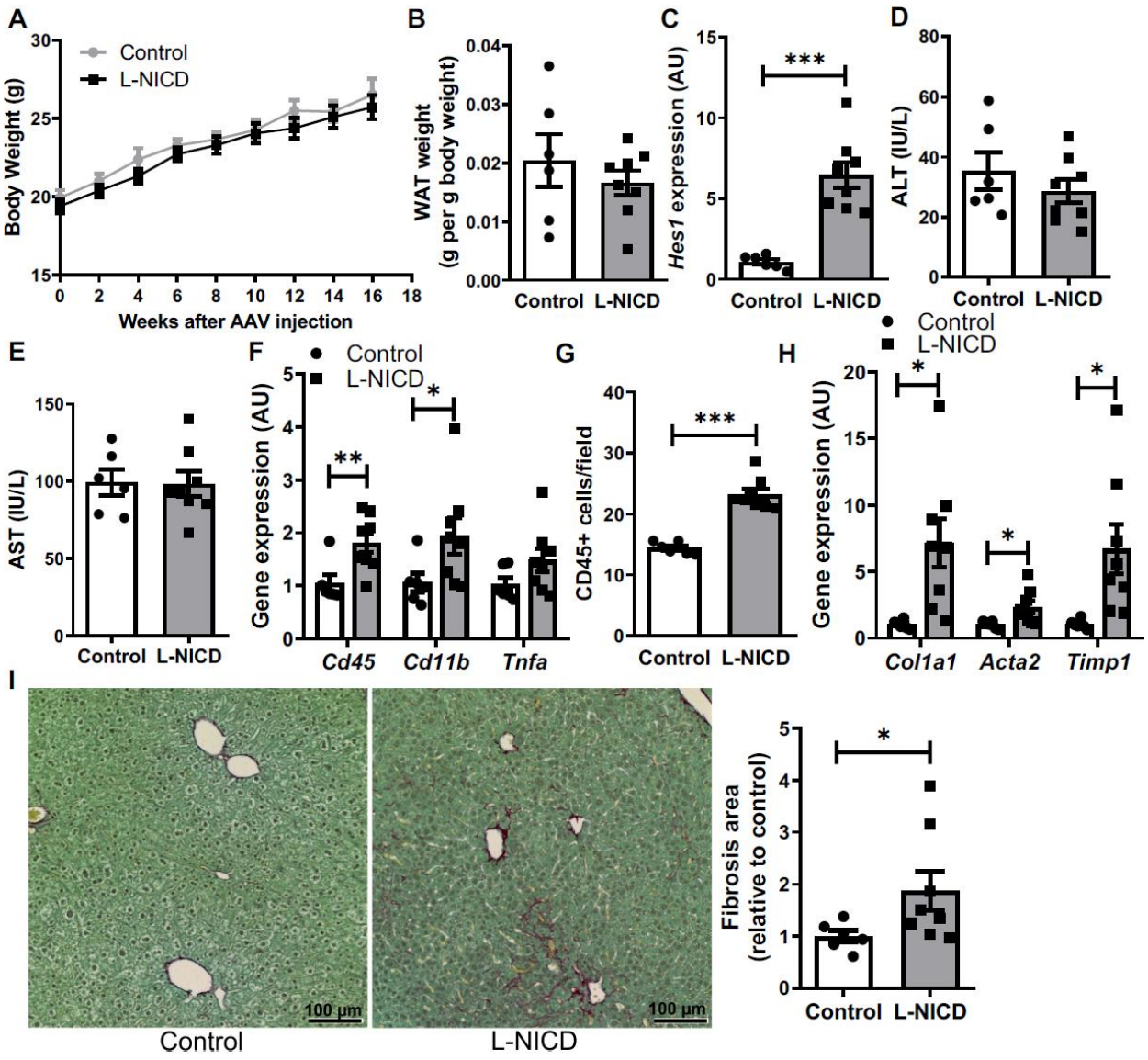

Fig. S9. **Characterization of chow-fed *L-NICD* female mice.** (**A**) Body weight curve, (**B**) epididymal WAT weight, (**C**) liver *Hes1*, (**D**) serum ALT and (**E**) AST, (**F**) liver inflammatory gene expression, (**G**) CD45+ cell infiltrate, (**H**) fibrogenic gene expression and (**I**) collagen deposition (scale bar, 100 μm) in chow-fed Cre- and *L-NICD* female mice (n = 7/group). *, $P < 0.05$, **, $P < 0.01$ and ***, $P < 0.001$ as compared to Cre- controls by 2-tailed *t* tests (2 groups). AU, arbitrary unit. All data are shown as the means ± s.e.m.

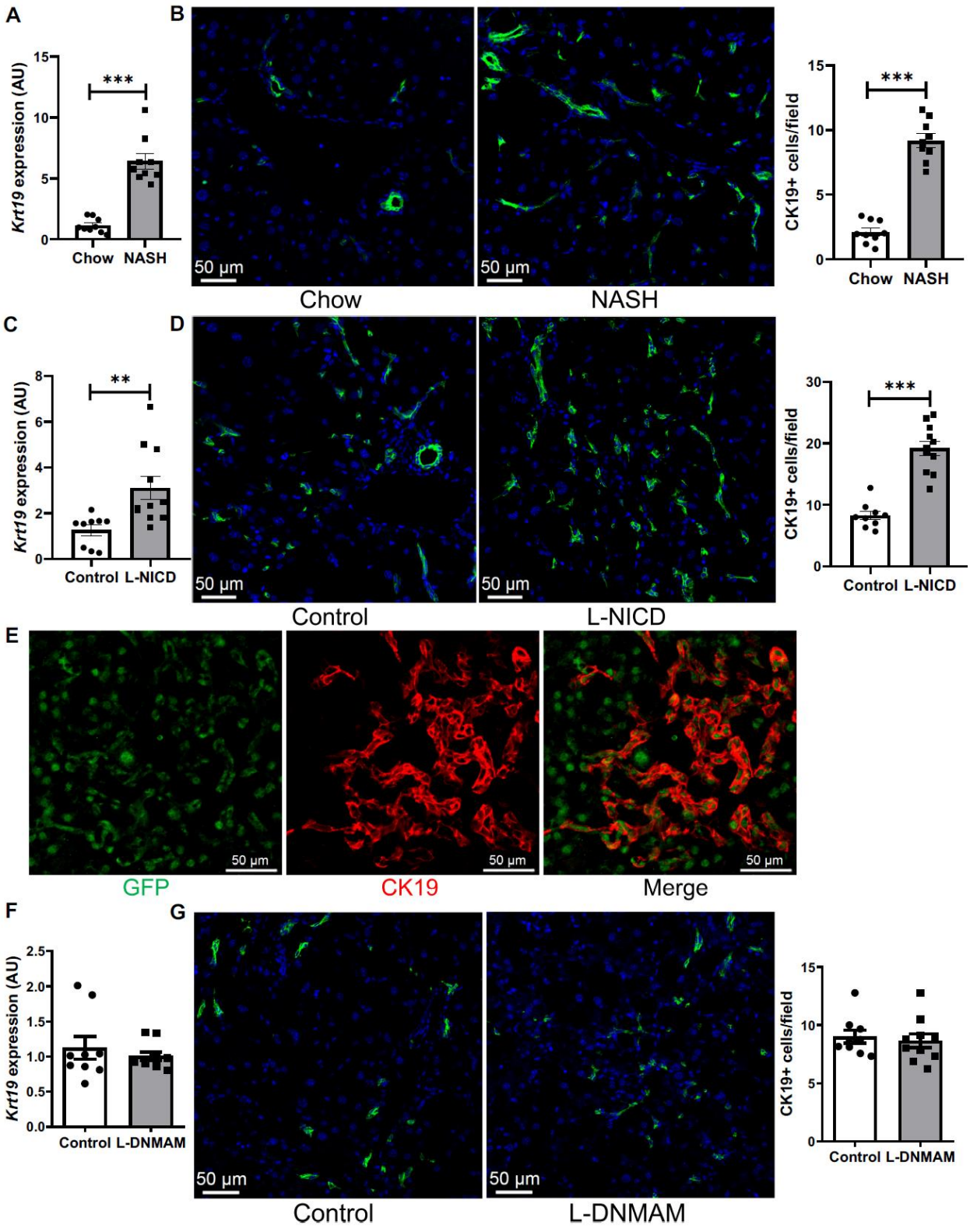

Fig. S10. **Loss of hepatocyte Notch activity does not affect ductular reactions.** (**A**) Liver *Krt19* expression and (**B**) CK19+ cells in WT mice fed NASH diet for 16 weeks (n = 9/group). (**C**) Liver *Krt19* expression and (**D**) CK19+ cells in Cre- and L-NICD mice fed NASH diet for 16 weeks (n = 9-11/group).

(**E**) Representative picture of hepatocyte-derived GFP+/CK19+ cholangiocytes in *L-NICD* mice. (**F**) Liver *Krt19* expression and (**G**) CK19+ cells in *L-DNMAM* mice fed NASH diet for 16 weeks (n = 9-10/group). *, $P < 0.05$, and ***, $P < 0.001$ as compared to the indicated controls by 2-tailed *t* tests (2 groups). Scale bar for all images, 50 μm. AU, arbitrary unit. All data are shown as the means ± s.e.m.

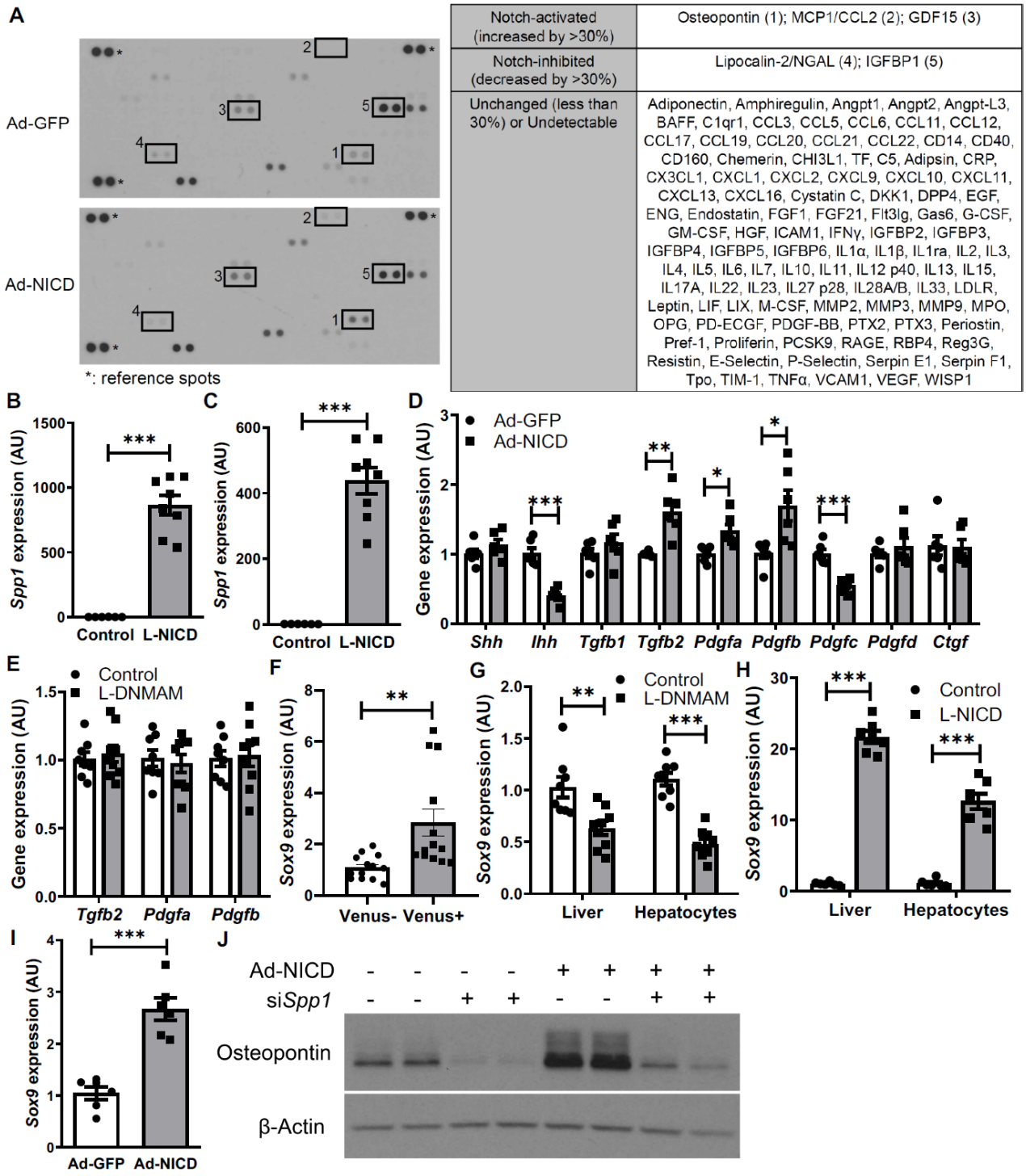

Fig. S11. **Hepatocyte Notch activity regulates *Spp1* and *Sox9* expression.** (**A**) Representative cytokine array of conditioned medium collected from control (Ad-GFP) and Ad-NICD-transduced primary hepatocytes (left) and all 111 cytokines examined in the array organized by Notch responsiveness (right). (**B**) Liver *Spp1* expression in chow-fed *L-NICD* male and (**C**) female mice (n = 6-8/group). (**D**) Expression of other fibrogenic factors in Ad-NICD-transduced hepatocytes (n =

6/group), with (**E**) confirmation of Notch-increased factors (from **Fig. S11D**) in hepatocytes isolated from NASH diet-fed *L-DNMAM* mice (n = 8/group). (**F** to **I**) *Sox9* expression in (**F**) Notch-inactive (Venus-) and Notch-active (Venus+) hepatocytes isolated from NASH diet-fed Notch reporter mice (n = 13/group), (**G**) livers and isolated hepatocytes from NASH diet-fed Cre- and *L-DNMAM* mice (n = 8/group), (**H**) livers and isolated hepatocytes from Cre- and *L-NICD* mice (n = 7/group) and (**I**) Ad-NICD-transduced WT mouse primary hepatocytes (n = 6/group). (**J**) Representative Western blots for Osteopontin protein in primary hepatocytes transfected with control siRNA or si*Spp1*. *p< 0.05, **p<0.01, ***p<0.001 as compared to the indicated controls by 2-tailed *t* tests (2 groups). NS, not significant. AU, arbitrary unit. Data are shown as the means ± s.e.m.

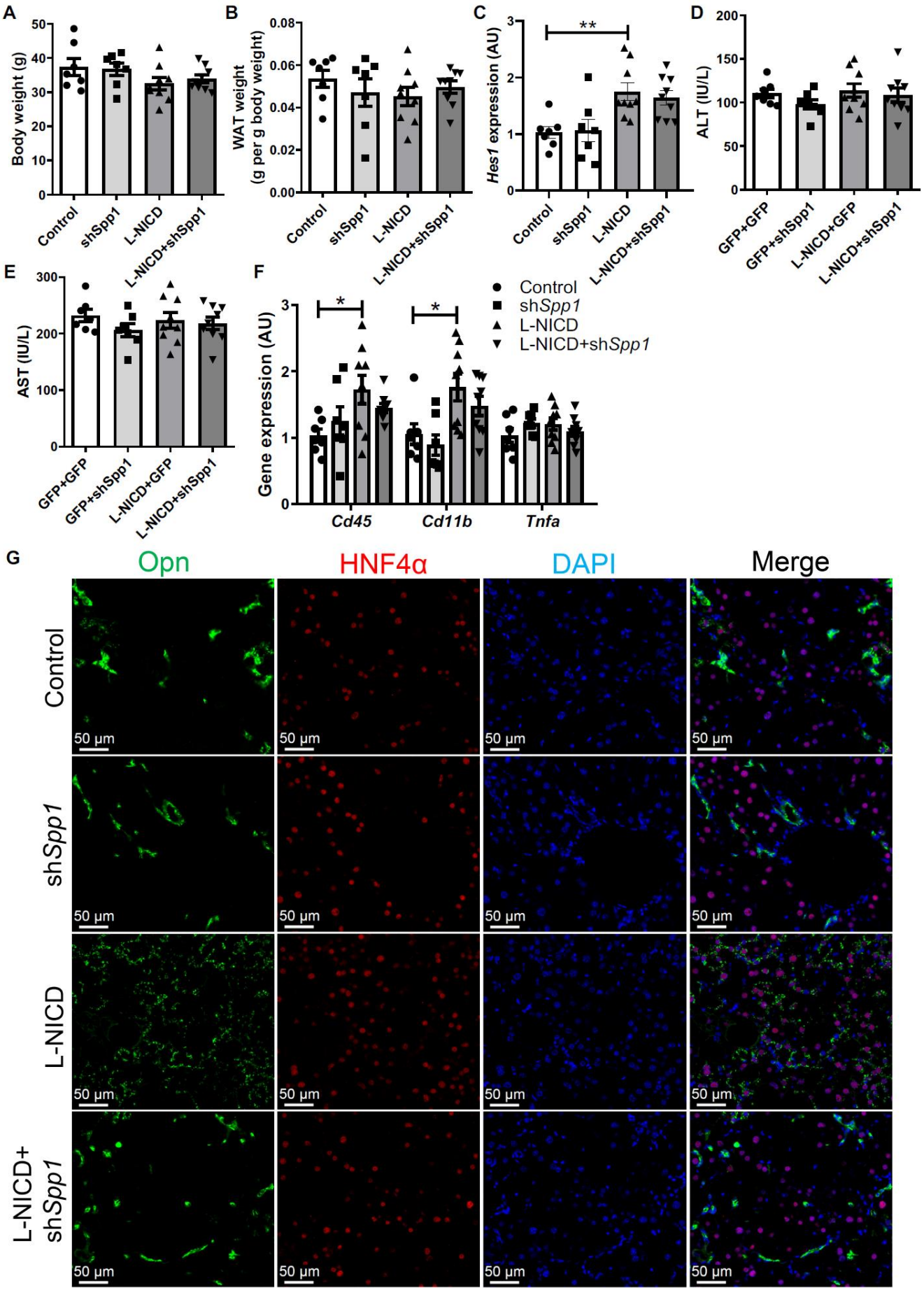
A
Body weight (g)
Control
shSpp1
L-NICD
L-NICD+shSpp1
B
WAT weight (g per g body weight)
C
Hes1 expression (AU)
**
D
ALT (IU/L)
GFP+GFP
GFP+shSpp1
L-NICD+GFP
L-NICD+shSpp1
E
AST (IU/L)
F
Gene expression (AU)
Control
shSpp1
L-NICD
L-NICD+shSpp1
*
*
Cd45
Cd11b
Tnfa
G
Opn
HNF4α
DAPI
Merge
Control
shSpp1
L-NICD
L-NICD+ shSpp1
50 μm

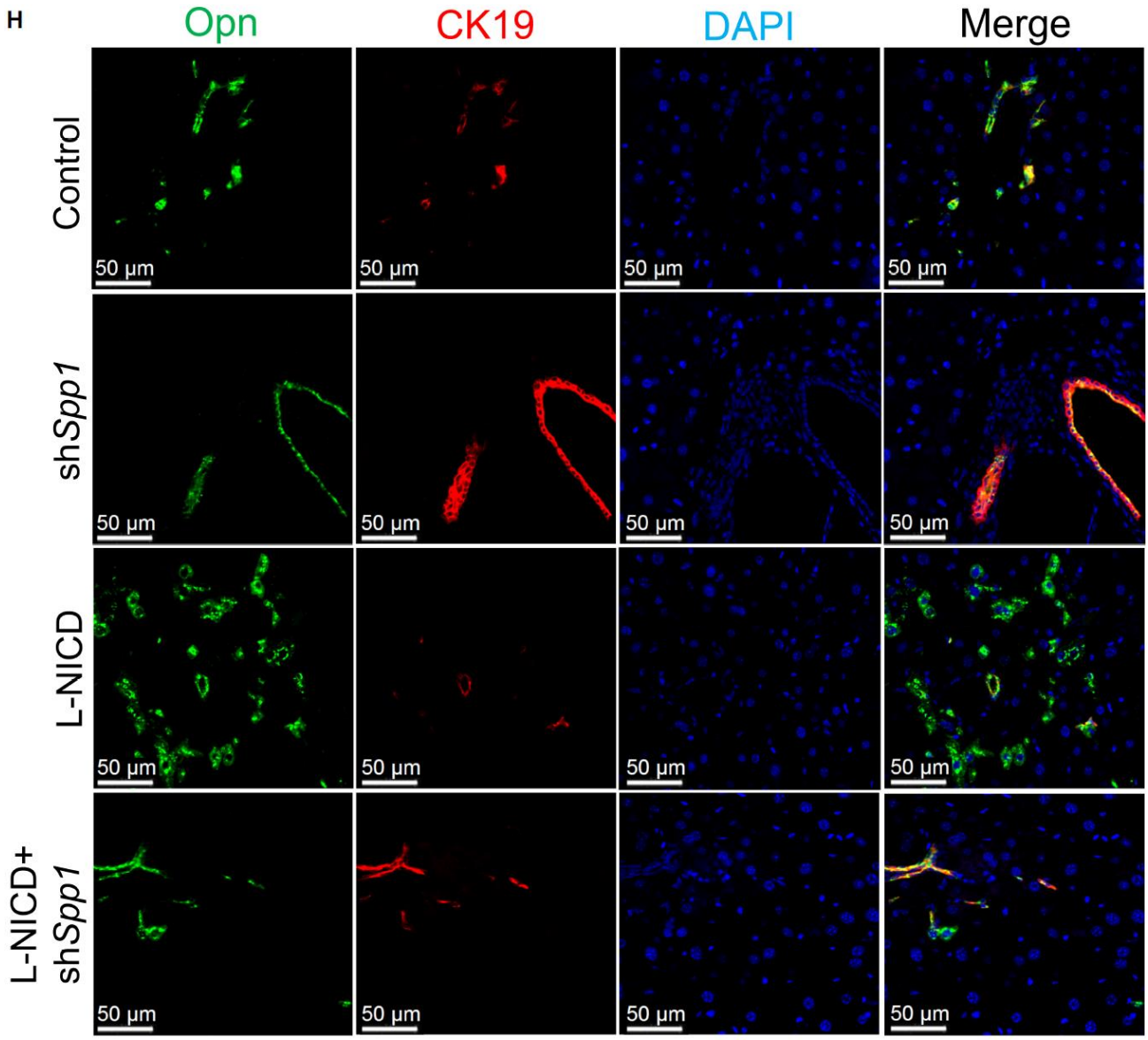

Fig. S12. **Characterization of AAV8-H1-sh*Spp1*-transduced mice.** (**A**) Body weight, (**B**) epididymal WAT weight, (**C**) liver Notch activity, (**D**) serum ALT and (**E**) AST, (**F**) liver inflammatory gene expression and (**G, H**) representative staining images from NASH diet-fed Cre- and L-NICD mice transduced with AAV8-H1-shControl or AAV8-H1-sh*Spp1* (n = 7-9/group). *, $P < 0.05$ and **, $P < 0.01$ as compared to the indicated controls by one-way ANOVA followed by post-hoc *t* tests (more than 2 groups). Scale bar for all images, 50 μm. AU, arbitrary unit. Data are shown as the means ± s.e.m.

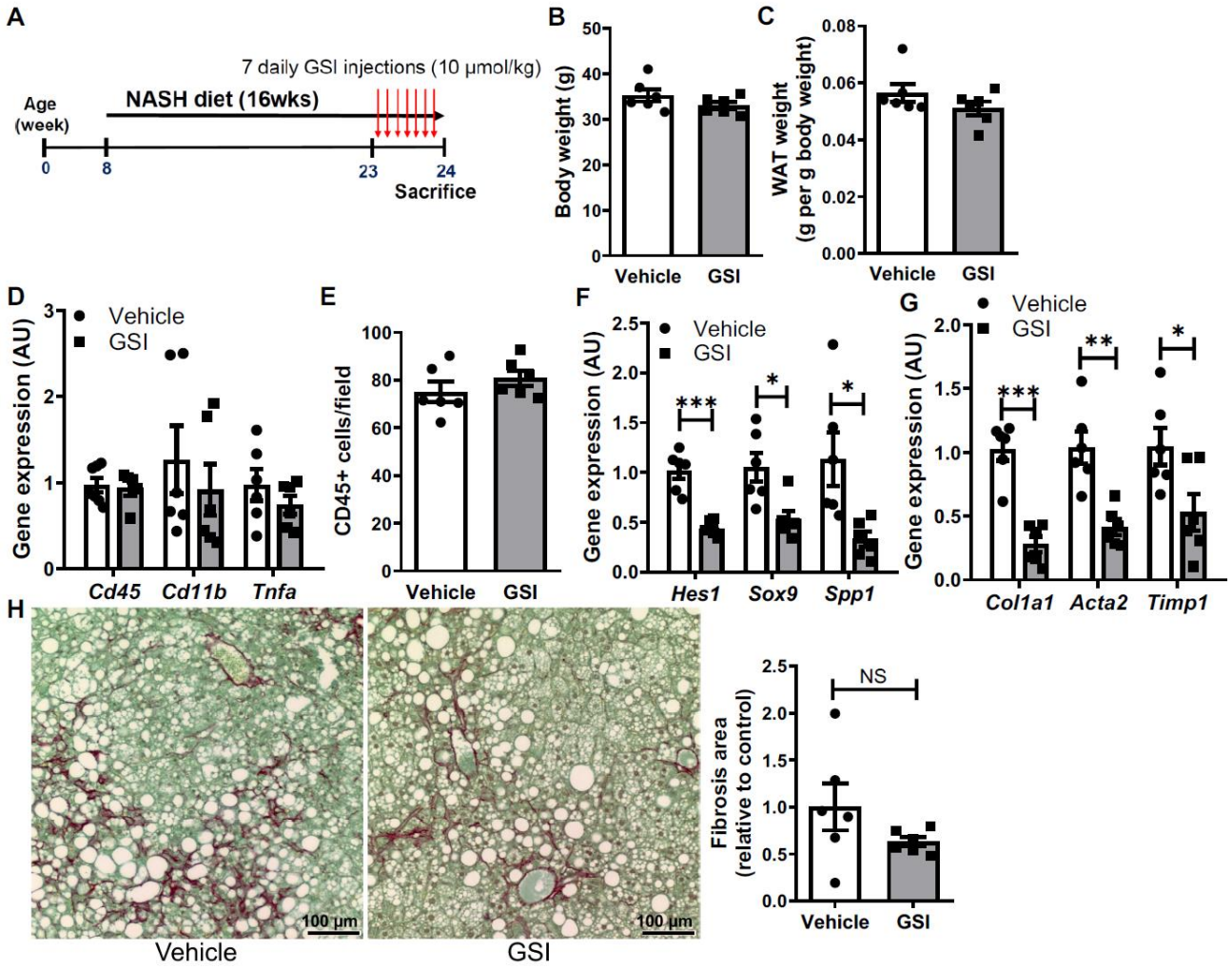

Fig. S13. **Characterization of GSI-treated, NASH diet-fed mice.** (**A**) WT mice were injected with vehicle or γ-secretase inhibitor (GSI) at 10 μmol/kg once daily for 1 week after 15 weeks of NASH-feeding. (**B**) Body weight, (**C**) epididymal WAT weight, (**D**) liver inflammatory gene expression, (**E**) CD45+ cell infiltrate, (**F**) Notch target and (**G**) fibrogenic gene expression and (**H**) liver collagen content (scale bar, 100 μm) in vehicle- and acute GSI-treated mice (n = 6/group). *, $P < 0.05$, **, $P < 0.01$ and ***, $P < 0.001$ as compared to vehicle-injected controls by 2-tailed *t* tests (2 groups). NS, not significant. AU, arbitrary unit. All data are shown as the means ± s.e.m.

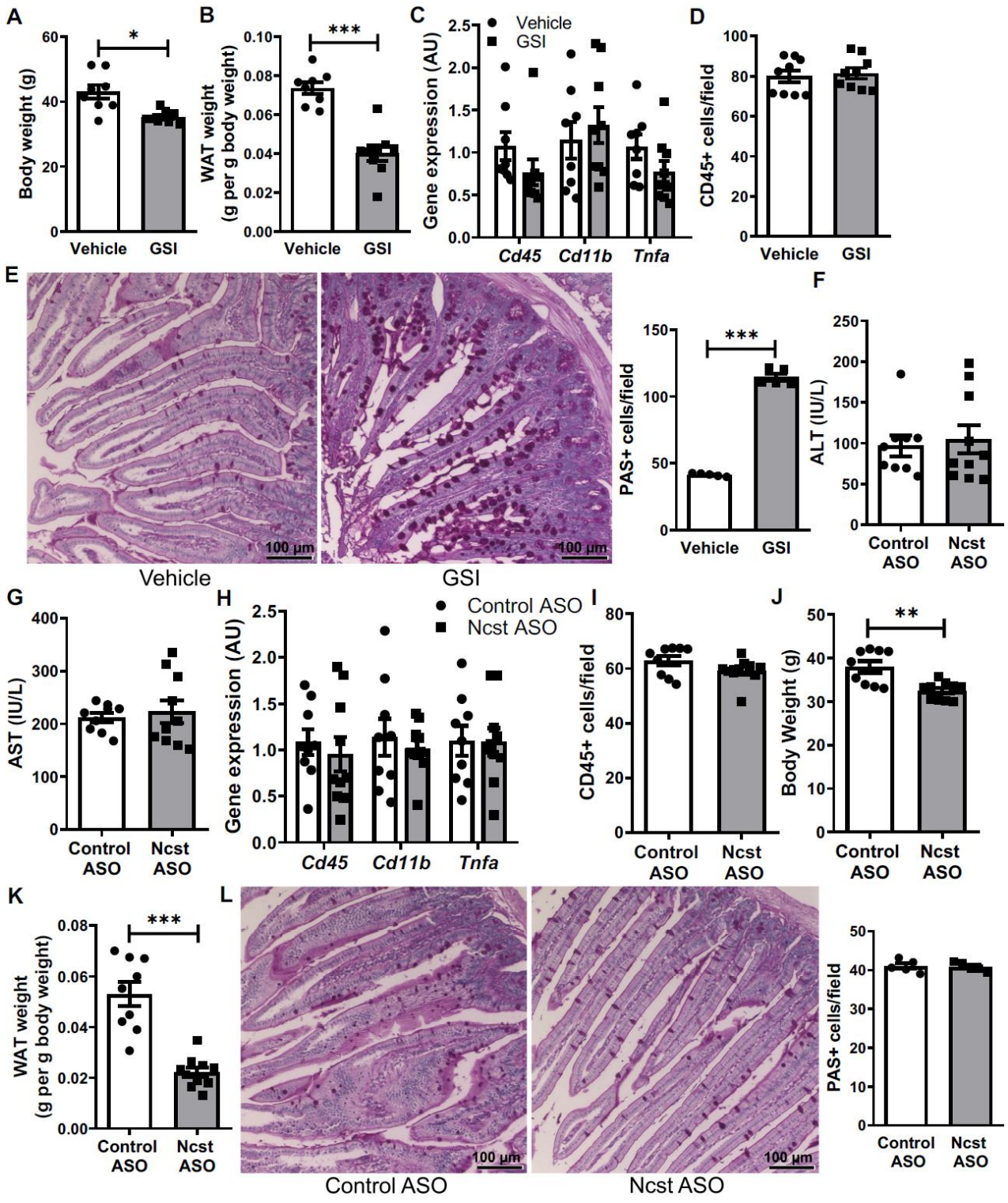

Fig. S14. **Characterization of GSI- and ASO-treated mice.** (**A**) Body weight, (**B**) epididymal WAT weight, (**C**) liver inflammatory gene expression and (**D**) CD45+ cell infiltrate in vehicle- and chronic GSI-treated NASH diet-fed WT mice (n = 8-9/group). (**E**) Goblet cell metaplasia, indicated by increased small intestine PAS staining with GSI treatment (n = 5/group). (**F**) Serum ALT and (**G**) AST, (**H**) liver

inflammatory gene expression and (**I**) CD45+ cell infiltrate, (**J**) body weight, (**K**) epididymal WAT weight in WT mice treated with either control or *Ncst* ASO (n = 9-10/group). (**L**) small intestine PAS staining with quantitation of intestinal goblet cell number in control or *Ncst* ASO-treated mice (n=5/group). *, $P < 0.05$ and ***, $P < 0.001$ as compared to the indicated controls by 2-tailed *t* tests (2 groups). Scale bar, 100 μm. AU, arbitrary unit. All data are shown as the means ± s.e.m.

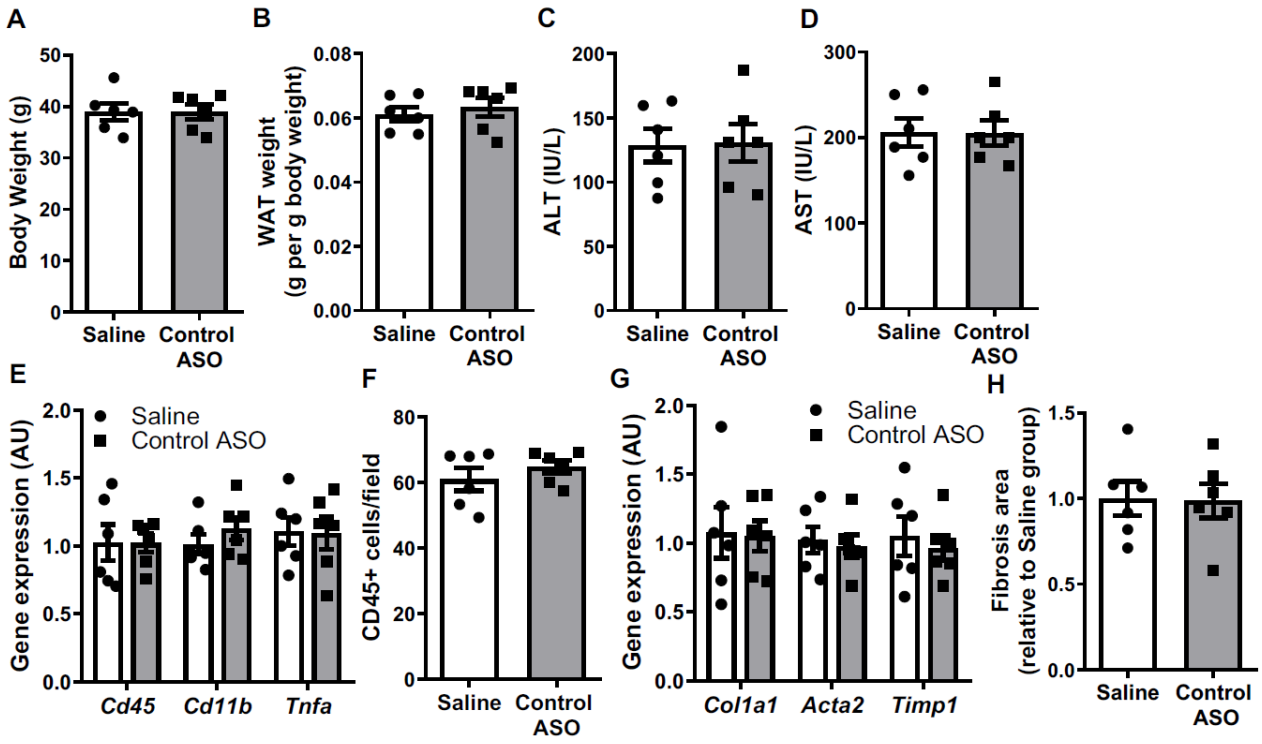

Fig. S15. **Comparison of saline- and control ASO-treated mice.** (**A**) Body weight, (**B**) epididymal WAT weight, (**C**) serum ALT and (**D**) AST, (**E**) liver inflammatory gene expression, (**F**) CD45+ cell infiltrate, (**G**) fibrogenic gene expression, and (**H**) liver collagen content in NASH diet-fed WT mice injected with saline and control ASO (25 mg/kg for 8 weeks), n = 6/group. 2-tailed *t* tests were performed to compare the two groups. AU, arbitrary unit. All data are shown as the means ± s.e.m.

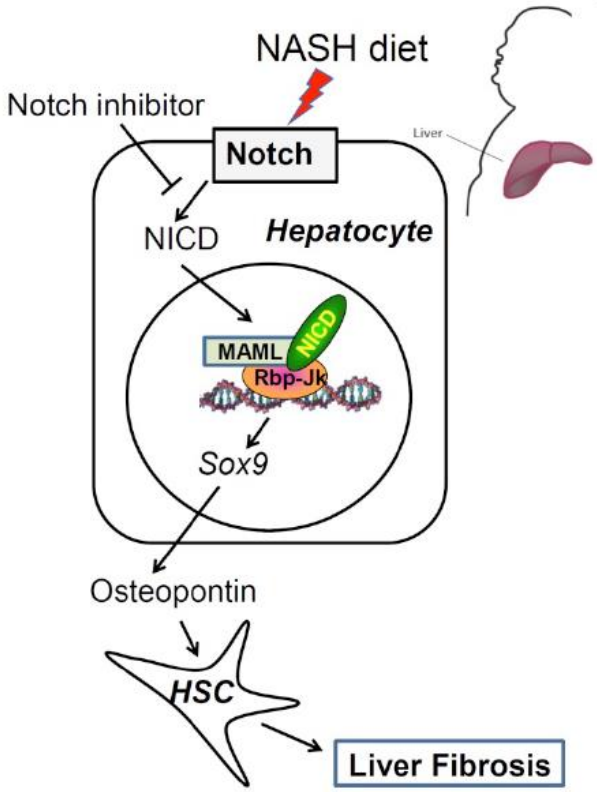

Fig. S16. **Model of hepatocyte Notch action to increase NASH-associated fibrosis.** Hepatocyte Notch is aberrantly activated in human and mouse NASH, which increases expression and secretion of Osteopontin via the Notch-responsive transcription factor Sox9. Osteopontin activates hepatic stellate cells (HSCs) and induces NASH-associated fibrosis that can be targeted by Notch inhibitors.

Table S1: Demographic and clinical features of PIVENS patients.

Cross-sectional study (n = 118, 72F/46M)			
	NR	R	*P*-value
Number	49	69	
Gender (female)	31	41	
Age (years)	46.9 ± 13.4	47.5 ± 12.0	0.786
BMI (kg/m^2)	36.3 ± 6.80	34.7 ± 7.42	0.238
NAS	4.84 ± 1.30	2.52 ± 1.09	$9.03*10^{-17}$
Fibrosis Score	1.71 ± 1.06	0.91 ± 1.13	$1.51*10^{-4}$
ALT (IU/L)	59.5 ± 28.1	36.1 ± 21.7	$5.24*10^{-6}$
HOMA-IR	6.07 ± 5.56	3.90 ± 2.78	0.0163

Longitudinal study (n = 21, 10F/11M)						
	Pre-treatment			End-of-treatment		
	NR	R	*P*-value	NR	R	*P*-value
Number	10	11		10	11	
Gender (female)	5	5		5	5	
BMI (kg/m^2)	37.3 ± 8.33	37.5 ± 9.55	0.952	38.3 ± 7.53	37.5 ± 8.93	0.829
NAS	4.10 ± 1.45	4.64 ± 1.43	0.405	4.80 ± 1.40	2.82 ± 0.874	0.00160
Fibrosis Score	1.40 ± 1.07	1.00 ± 1.18	0.427	1.60 ± 0.843	0.55 ± 0.934	0.0136
ALT (IU/L)	82.8 ± 58.7	86.6 ± 56.7	0.881	67.4 ± 23.1	40.1 ± 21.1	0.0112
HOMA-IR	5.00 ± 2.37	5.54 ± 3.65	0.693	4.85 ± 3.02	4.44 ± 3.06	0.768

Values are means ± SD. F: female; M: male; NR: non-responders; R: responders; BMI: body mass index; NAS: NALFD activity score; HOMA-IR: homeostatic model assessment of insulin resistance. *P*-values were generated by two-tailed Student's *t*-test between NR and R groups.

Table S2: **Demographic and clinical features of cross-sectional cohort of patients with suspected NASH.**

	Biopsy cohort (N = 159)
Age, years	45 ± 10
Sex, female	95 (60%)
BMI, Kg/m^2	37.8 ± 8.5
IFG/T2DM	41 (26%)
Glucose, mmol/l	5.6 ± 1.8
Total cholesterol, mmol/l	5.3 ± 1.0
LDL cholesterol, mmol/l	3.2 ± 1.0
HDL cholesterol, mmol/l	1.3 ± 0.4
Triglycerides, mmol/l	1.6 ± 1.0
ALT, IU/l	28 [18-57]
AST, IU/l	22 [17-33]

Values are means ± S.D., median [interquartile range], or number (%). BMI: body mass index; IFG: impaired fasting glucose; T2DM: type 2 diabetes mellitus; LDL: low-density lipoprotein; HDL: high-density lipoprotein.

Table S3. Sequences of qPCR primers used in the experiments.

Gene	Primers
18S forward (human)	5'-AAACGGCTACCACATCCAAG-3'
18S reverse (human)	5'-CCTCCAATGGATCCTCGTTA-3'
ACTB forward (human)	5'-AAGAGCTACGAGCTGCCTGA-3'
ACTB reverse (human)	5'-TCCATGCCCAGGAAGGAAGG-3'
HES1 forward (human)	5'-CAACACGACACCGGATAAACCA-3'
HES1 reverse (human)	5'-TGCCGCGAGCTATCTTTCTTC-3'
HEYL forward (human)	5'-AGCCTGCGTTCGCCATGAA-3'
HEYL reverse (human)	5'-CTATGATCCCTCTGCGTTTCTTCC-3'
SPP1 forward (human)	5'-TTGCAGCCTTCTCAGCCAAA-3'
SPP1 reverse (human)	5'-CAGCCTGTTTAACTGGTATGGCAC-3'
36b4 forward (mouse)	5'-GGAGAAACTGCTGCCTCACA-3'
36b4 reverse (mouse)	5'-AGCAGCTGGCACCTTATTGG-3'
Acta2 forward (mouse)	5'-CAGCCATCTTTCATTGGGATGGAG-3'
Acta2 reverse (mouse)	5'-AATGCCTGGGTACATGGTGG-3'
Cd11b forward (mouse)	5'-CTCACGTATCCGTGCCTTCTT-3'
Cd11b reverse (mouse)	5'-GTCCACGCAGTCCGGTAAA-3'
Cd45 forward (mouse)	5'-ACTGAGCACAACAGAGAATGCC-3'
Cd45 reverse (mouse)	5'-AGCGTGGATAACACACCTGGA-3'
Col1a1 forward (mouse)	5'-GAACTGGACTGTCCCAACCC-3'
Col1a1 reverse (mouse)	5'-TTGGGTCCCTCGACTCCTAC-3'
Ctgf forward (mouse)	5'-AGAACTGTGTACGGAGCGTG-3'
Ctgf reverse (mouse)	5'-GGTGCACCATCTTTGGCAGT-3'
Hes1 forward (mouse)	5'-ACGACACCGGACAAACCAAA-3'
Hes1 reverse (mouse)	5'-GAATGCCGGGAGCTATCTTTCT-3'
Ihh forward (mouse)	5'-ACCTCAGACCGTGACCGAAA-3'
Ihh reverse (mouse)	5'-GGCCGAATGCTCAGACTTGAC-3'
Krt19 forward (mouse)	5'-AGTCCCAGCTCAGCATGAAAG-3'
Krt19 reverse (mouse)	5'-CAGCTGGACTCCATAACGGG-3'
Nicastrin forward (mouse)	5'-AATGGAGAAGCTGAAGGGAAC-3'
Nicastrin reverse (mouse)	5'-CCCGTAGGAGTTGGAGTAAATAC-3'
Notch1 forward (mouse)	5'-CAGACCAACACGCAGTACCA-3'
Notch1 reverse (mouse)	5'-GACGTCAATGCCTCGCTTCT-3'
Notch2 forward (mouse)	5'-GCTATGGCCAACAGTAACCCT-3'
Notch2 reverse (mouse)	5'-GCGTAGCCCTTCAGACACTC-3'
Notch3 forward (mouse)	5'-TGTGCTACAGCCGTGTGTTT-3'
Notch3 reverse (mouse)	5'-CACAAGAGGCCTGTCTTCCC-3'
Notch4 forward (mouse)	5'-ACCAGAGAGCTTCTGTGTGGAG-3'
Notch4 reverse (mouse)	5'-CACTGGCAGATCCCTTGTCC-3'
Pdgfa forward (mouse)	5'-GAGGAGGAGACAGATGTGAGGT-3'
Pdgfa reverse (mouse)	5'-GAACAAAGACCGCACGCAC-3'
Pdgfb forward (mouse)	5'-TGCACAGAGACTCCGTAGATGA-3'

Pdgfb reverse (mouse)	5’-CACTCGGCGATTACAGCAGG-3’
Pdgfc forward (mouse)	5’-CCAGTCAGCCAAATGCTCCT-3’
Pdgfc reverse (mouse)	5’-GGATCTTGCACTCCGTTCTGT-3’
Pdgfd forward (mouse)	5’-AACCTCAGGAGAGATGAGAGCA-3’
Pdgfd reverse (mouse)	5’-AGCCACCATGTCAGAAGCAG-3’
Shh forward (mouse)	5’-CAACGTAGCCGAGAAGACCC-3’
Shh reverse (mouse)	5’-TGCACCTCTGAGTCATCAGCC-3’
Sox9 forward (mouse)	5’-TCTGGAGGCTGCTGAACGAG-3’
Sox9 reverse (mouse)	5’-GCTTGTCCGTTCTTCACCGA-3’
Spp1 forward (mouse)	5’-CCTGGCTGAATTCTGAGGGAC-3’
Spp1 reverse (mouse)	5’-CAGTCACTTTCACCGGGAGG-3’
Tbp forward (mouse)	5’-CACAGGAGCCAAGAGTGAAGAA-3’
Tbp reverse (mouse)	5’-GCCTTCCAGCCTTATAGGGAAC-3’
Tgfb1 forward (mouse)	5’-GCCCGAAGCGGACTACTATG-3’
Tgfb1 reverse (mouse)	5’-ATAGATGGCGTTGTTGCGGT-3’
Tgfb2 forward (mouse)	5’-ATAATTGCTGCCTTCGCCCTC-3’
Tgfb2 reverse (mouse)	5’-AGGCTGAGGACTTTGGTGTGT-3’
Timp1 forward (mouse)	5’-ACTCGGACCTGGTCATAAGGG-3’
Timp1 reverse (mouse)	5’-CGCTGGTATAAGGTGGTCTCGT-3’
Tnfa forward (mouse)	5’-CCCACGTCGTAGCAAACCA-3’
Tnfa reverse (mouse)	5’-TCTTTGAGATCCATGCCGTTGG-3’